國立交通大學

多媒體工程研究所

碩 士 論 文

基於圖形處理器之即時熱影像模擬

GPU-based Real-Time Simulation of Thermogrphy

研　究　生：邱晟瑋

指導教授：林奕成　博士

中 華 民 國 九十九 年 七 月

基於圖形處理器之即時熱影像模擬

GPU-based Real-Time Simulation of Thermogrphy

研 究 生：邱晟瑋　　　　Student：Cheng-Wei Chiu

指導教授：林奕成　　　　Advisor：Dr. I-Chen Lin

國 立 交 通 大 學

多 媒 體 工 程 研 究 所

碩 士 論 文

A Thesis

Submitted to Institute of Multimedia Engineering

College of Computer Science

National Chiao Tung University

in partial Fulfillment of the Requirements

for the Degree of

Master

in

Computer Science

July 2010

Hsinchu, Taiwan, Republic of China

中華民國九十九年七月

基於圖形處理器之即時熱影像模擬

研究生：邱晟瑋　　指導教授：林奕成　博士

國立交通大學

多媒體工程研究所

摘要

本論文針對熱式影像為目標，提出一套基於圖形處理器之即時熱影像模擬演算法。我們從熱力學定律中推導出的熱傳遞模型，藉而模擬真實的熱式影像。由於傳統的熱模擬注重精密的數值計算，模擬的過程往往花費了過多的時間。因此，我們建立了簡化後的熱傳遞模型，並使用有限元素法來描述物體的動態熱能，最後藉由圖形處理器的平行運算能力加速模擬流程，輸出即時擬真的熱影像。其中，我們以 Phong 反射模型為主模擬熱輻射的變化，並以較少的儲存空間計算均勻材質實心物體的熱傳導過程，以圓柱體受風力的熱對流影響簡化時寄物體的複雜邊界。最後，我們將比較實驗結果，分析出模擬過程中最合適的各項參數。

關鍵字：熱影像模擬、光反射模型、虛擬實境

GPU-based Real-time Simulation of Thermography

Student: Cheng-Wei Chiu **Advisor: Dr. I-Chen Lin**

Institute of Multimedia Engineering

National Chiao Tung University

Abstract

The goal of this thesis is to propose an efficient framework for real-time thermography simulation. Since our purpose is not fully physical simulation but visually correct thermographic view, we propose a plausible illumination method for approximation of heat transfer where radiation, conduction and convection are all included. We use Phong illumination model to simulate radiation since indirect reflection can be ignored with low temperature difference. For simulation of conduction, we construct less 2D textures to substitute a large-sized volumetric 3D object to reduce computational complexity of heat propagation. To simulate convectional effect, we simplify the shapes of objects into cylindrical case and apply the formula of heat transfer from a cylinder in cross flow. All of these methods are able to be accelerated by GPU-based rendering which synthesizes realistic thermal images of a virtual environment in real-time.

Keywords: thermal image, illumination model, virtual reality

Acknowledge

First of all, I would like to thank my advisor, Dr. I-Chen Lin, for his guidance in the past two years. Also, I appreciate all members of Computer Animation & Interactive Graphics Lab for their help and push. And last, I am grateful to my family for their support and encouragement

Contents

List of Figure

List of Table

1. Introduction

1.1 Motivation

To acquire more clear images from dim or dark environment, we have to utilize specific sensors to enhance dim images or visualize signals besides visible light spectrums. Thermal image device is the one of most pervasively used sensor for such purposes in military or secure usages.

Thermography is a type of infrared imaging science. Thermographic cameras detect radiation in the infrared range of the electromagnetic spectrum and visualize the received radiation. Since infrared radiation is emitted by all objects, according to the black body radiation law, thermography allows one to see variations in temperature. When viewed by a thermographic camera, warm objects are much more conspicuous than cooler backgrounds. Therefore, humans and other warm-blooded animals become easily visible against the environment, in either day or night. As a result, thermography are extensive used for uncover humans or vehicles in military or security purposes. Besides, it is also helpful for other usages. For instance, firefighters use it to see through smoke, find persons, and localize the base of a fire. With thermal imaging, power-lines-maintenance technicians locate overheating joints and parts, a sign of their failure, to avoid potential hazards.

However, it is expensive and risky to train novices in invisible environments. One of the practical substitutions is training the novices in a virtual environment where thermography is simulated. This environment is controllable to decrease danger and costly hardware; it also provide realistic visual experience.

The goal of this thesis is to propose an efficient framework for real-time thermography simulation. Since the views of environments by thermograhpic camera are due to variations in temperature, we simulate the heat transfer system to visualize temperature information from synthetic environments, which includes a plausible illumination model for approximation of physical heat transfer. While completely performing the detail of theory of heat transfer is computationally intensive, the goal of this simulation focus on rendering visually realistic thermal images instead of exactly implementing all the formulas of heat transfer system.

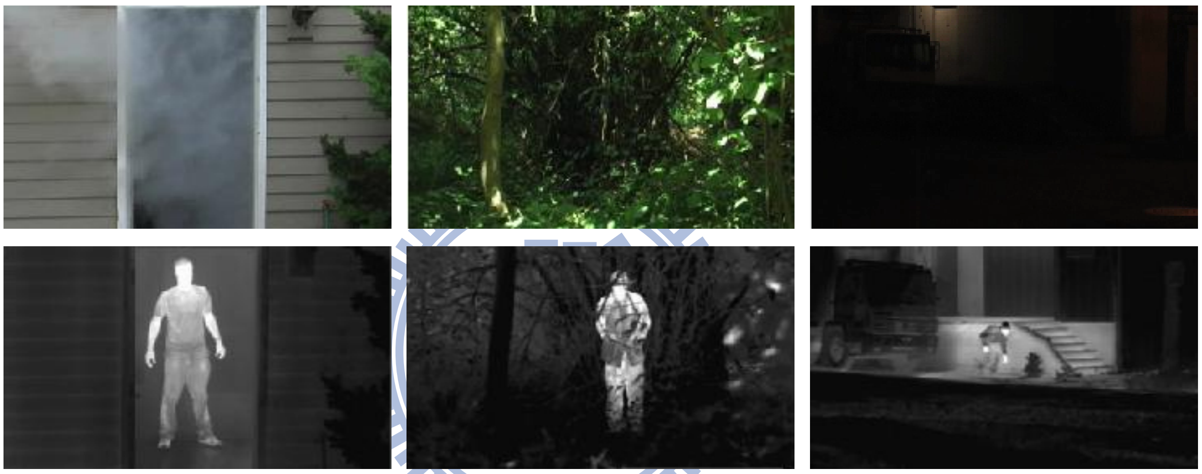

(a) **(b)** **(c)**

Figure 1.1 Normal visions and thermal images. (a) Through smoke in daylight. (b) Through foliage in daylight. (c) Through shadow at night [PR].

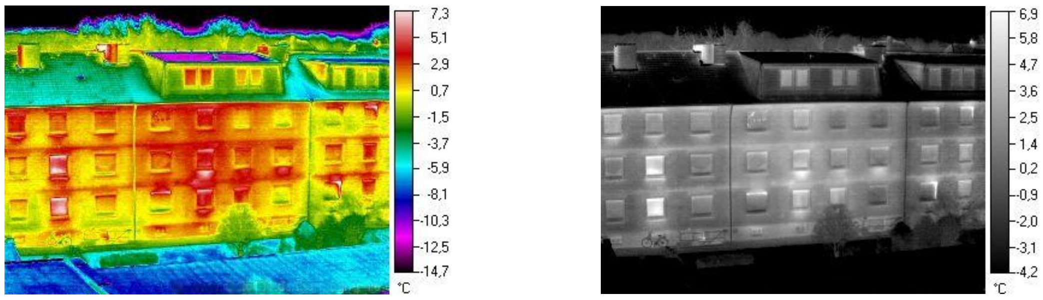

Figure 1.2 Thermal image of houses which display heat radiation in color and black-and-white [Thermal Image].

1.2 Background

When an object or fluid is at a different temperature from its surroundings, transfer of thermal energy, also known as heat transfer, or heat exchange, occurs in such a way that the body and the surroundings gradually reach thermal equilibrium. Heat transfer always occurs from a higher-temperature object to a cooler-temperature one as described by the second law of thermodynamics. Where there is a temperature difference between objects in proximity, heat transfer between them can never be stopped; it can only be slowed. In this simulation system, all methods of heat transfer also repeatedly calculate the variation of heat. The heat transfer methods comprise three types of phenomena: radiation, conduction and convection.

Radiation:

All objects with a temperature above the absolute zero radiate energy at a rate equal to their emissivity multiplied by the rate at which energy would radiate from them if they were a black body. No medium is necessary for radiation to occur, since it is transferred through electromagnetic waves. By comparing traditional graphics and infrared image shown as Table 1.1, we know that the critical difference is range of wave-band. If we replace reflection coefficients by thermal reflection coefficients in traditional graphics rendering, we can get same result of thermal image.

Table 1.1 Comparison between traditional graphics and infrared images.

	Traditional graphics	Infrared images
For Human Eyes	Visible	Invisible
Received Wave-band	0.38～0.76μm	>0.76μm
Intensity Representation	RGB channel	Single channel (Grayscale)

The radiosity [GTGB84] method is used to solve for the radiative heat transfer between numbers of surfaces. This method is also applied in 3D computer graphics for global illumination rendering. Vice versa, these algorithms of global illumination [Land02, ZIK98, Bunn05] can solve for the radiative heat transfer as well. However, most radiosity-based algorithms make use of iterative light transfer calculations which is of high computation cost. On the other hand image-space algorithms [DS05, Mitt07 and RGS09] can be an efficient approximation of global illumination. Though these approximation methods are of high computational efficiency, it may not provide all required effects.

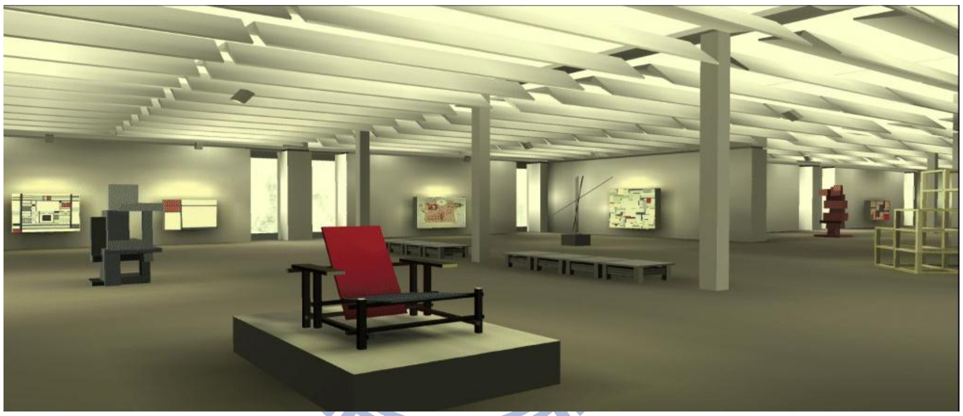

Figure 1.3 Radiosity method using in global illumination [PCG].

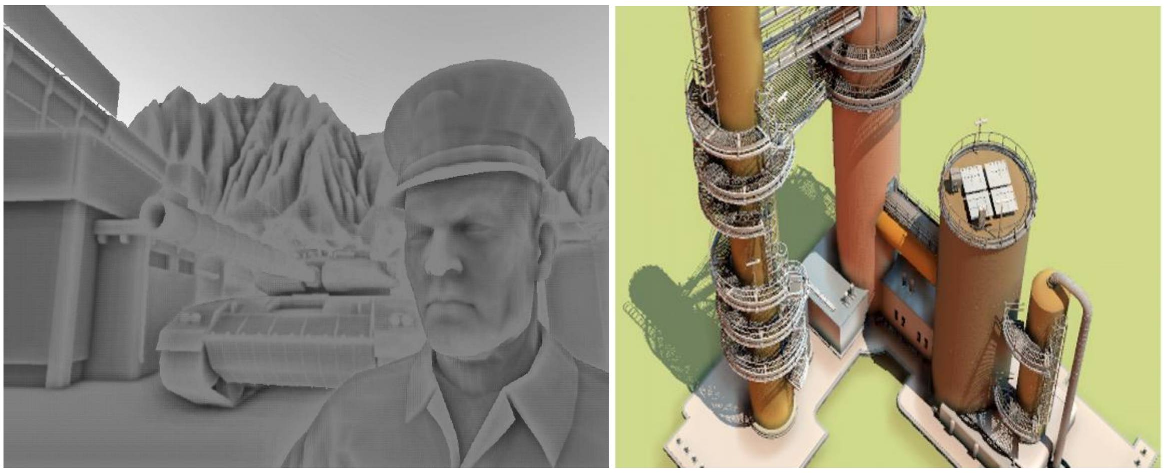

Figure 1.4 Image-based algorithms, Screen Space Ambient Occlusion (SSAO) and Directional Occlusion (SSDO) [Mitt07, RGS09].

Conduction:

Conduction is the transfer of heat from one molecule of matter to another. Conduction is greater in solids, where atoms are in constant contact. In liquids (except liquid metals) and gases, the molecules are usually further apart, giving a lower chance of molecules colliding and passing on thermal energy.

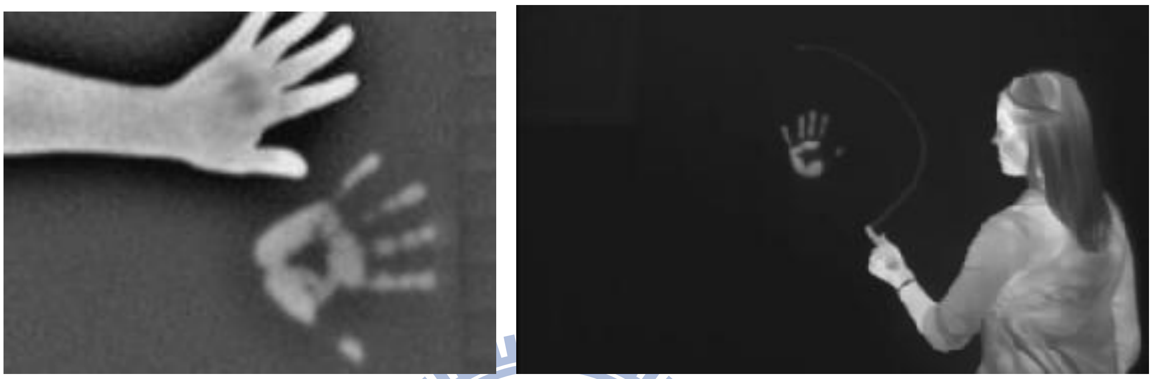

Figure 1.5 Thermal image of hand print on wall [PR].

To simulate the conduction phenomena, molecular dynamic (MD) methods are generally accepted means for simulating molecular scale models of matter. Objects and time step of simulation should be divided as tiny as well to describe the technique as a “virtual microscope” with high temporal and spatial resolution. Besides, conduction between dynamic objects should consider whether there’re surface contacts. That means the relation of connection changed during the movements in scene. There are two main categories of collision detection, object-based [KHMS*98] and image-space-based [BWS99] algorithm. The object-based collision detection computes the bounding volumes of objects in 3D scene. The image-based collision detection only computes the data of rendered images (e.g. depth value or color value). The weakness of object-based collision detection is its computational complexity. When complexity of the scene is complicated, the computing time will increase since our target is for flight or vehicle simulation.

Convection:

Convection is the movement of molecules within fluids (i.e. liquids and gases). As the fluid moves quicker, the convective heat transfer increases. Nevertheless, the presence of bulk motion of the fluid also enhances the heat transfer between the solid surface and the fluid. For example, an ice cube melts faster when it is blown in the wind.

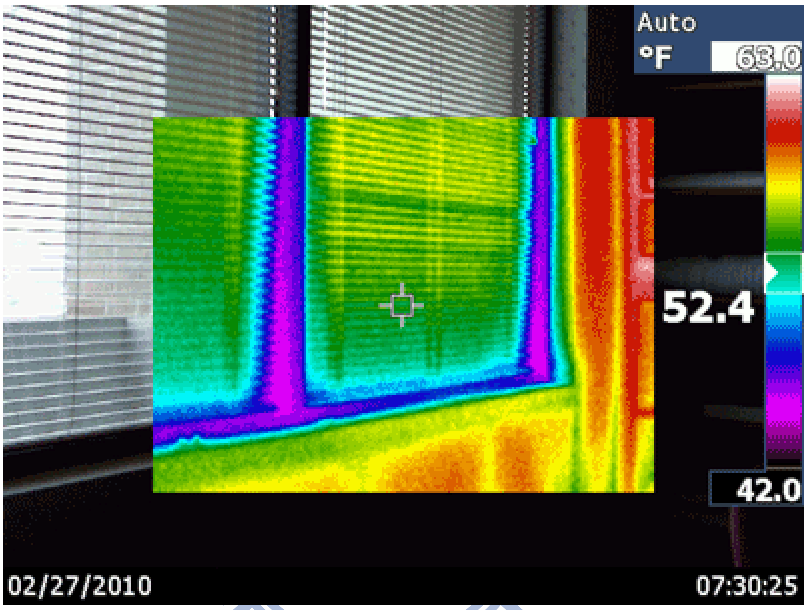

Figure 1.6 Thermal image of heat loss around windows by thermal convection.

According to the definition of computational fluid dynamics (CFD), numerical methods can be used to solve and analyze problems that involve fluid flows. While apply full CFD for convection, it requires the millions of calculations to simulate the interaction of liquids and gases with surfaces defined by boundary conditions. Lattice Boltzmann method (LBM) is a class of CFD methods for fluid simulation. It solves the conservation equations of macroscopic properties numerically unlike the traditional CFD methods. LBM models the fluid consisting of fictive particles which perform consecutive propagation and collision processes over a discrete lattice mesh. Due to its particulate characteristic, LBM takes advantages in dealing with complex boundaries, incorporating of microscopic interactions, and parallelization of the algorithm. However, this method does not support simulating incompressible flow such as gas and high-speed fluid.

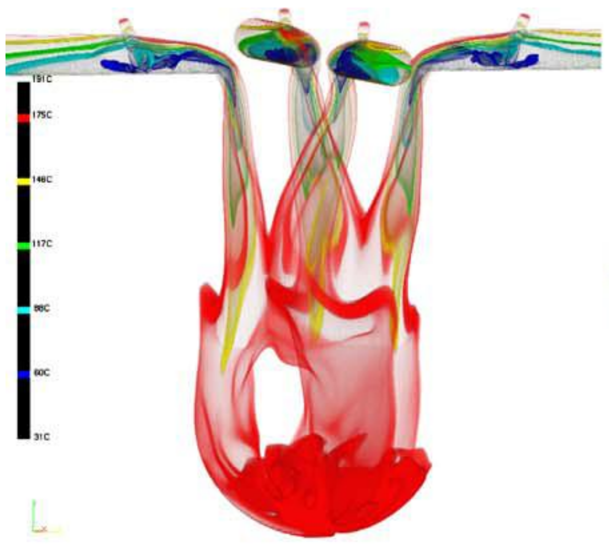

Figure 1.7 Visual simulation of thermal fluid dynamics in a pressurized water reactor [FKZQ*09].

1.3 Framework

In this thesis, we present an approximation of heat transfer system which consists of radiation, conduction, convection and producing visually similar thermal image. The process includes two main steps:

1. **Voxelization for 3D Model**. Since the temperatures between various parts of object may not be the same, we use the finite element method to visualize temperature of object in detail. For this purpose, we separate surface of object model in orthogonal views and store geometric information to a series of textures. By this step, an object model can be represented as numerous voxels.
2. **Simulation of Heat Transfer**. Voxelized objects exchange heat with other voxels in contact and strong heat sources. We consider wind blowing to make quickly temperature

equilibrium of objects and environment. The voxelization textures store heat energy and update in parallel through GPU calculation. Finally, we render objects with stored heat in textures and reflected heat of radiation on surface in screen.

To make our simulation efficient, we propose a GPU-liable visualization system. All of these methods are able to be accelerated by GPU-based rendering which synthesizes realistic thermal images of a virtual environment in real-time.

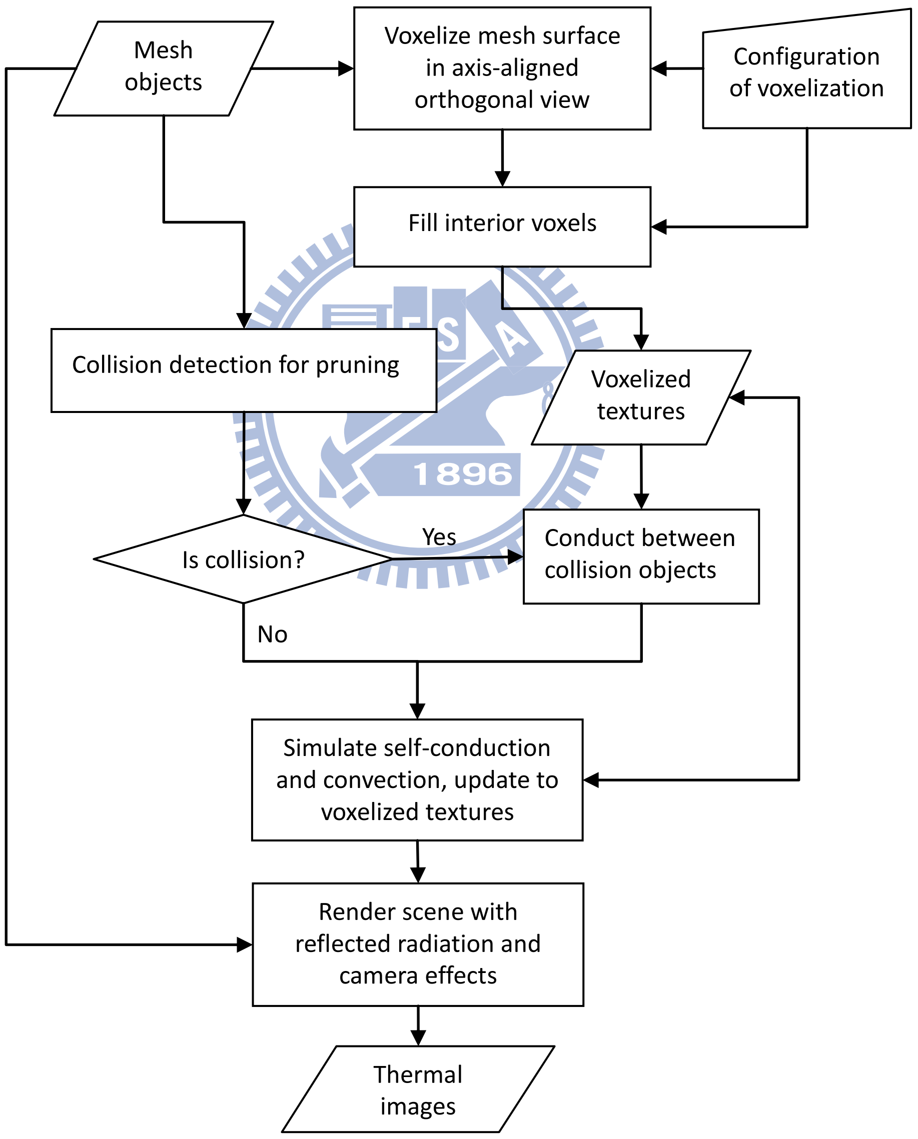
Mesh objects
Voxelize mesh surface in axis-aligned orthogonal view
Configuration of voxelization
Fill interior voxels
Collision detection for pruning
Voxelized textures
Is collision?
Yes
No
Conduct between collision objects
Simulate self-conduction and convection, update to voxelized textures
Render scene with reflected radiation and camera effects
Thermal images

Figure 1.8 The flow chart of the proposed system of synthesis thermal images.

2. Related Work

Infrared Image Synthesis. C. Garnier et al. [GCFM*99] described an IR sensor model developed from study of physical effects involved in IR image acquisition process. Their approach consists of a combination and an extension of current camera models used in visible and infrared image synthesis, and they also merges ray tracing and post-processing techniques. Zhangye Wang et al. [WWBP01] established an infrared model for ground targets, such as tank. They considered the effect of inner heat source, friction and various environmental factors and drew infrared images of target at various states by the Computer Graphics techniques. Zhangye Wang et al. [WPLJ01] and Zhaoyi Jiang et al. [JWJP04] proposed new IR image synthesis model accounting for meteorological, environmental, material and artificial factors. The energy equilibrium equation is built based on the principle of heat transfer and infrared physics and a finite difference method is adopted to solve the equations. Zhaoyi Jiang et al. [JWP03] proposed a method to constitute the dynamic infrared scene by combining scene geometric modeling with multi-spectral image. Multi-spectral IR textures are correspondent to materials of object surface. The actual attenuated IR radiation intensity is expressed by Phong illumination model between 10℃ and 50℃.

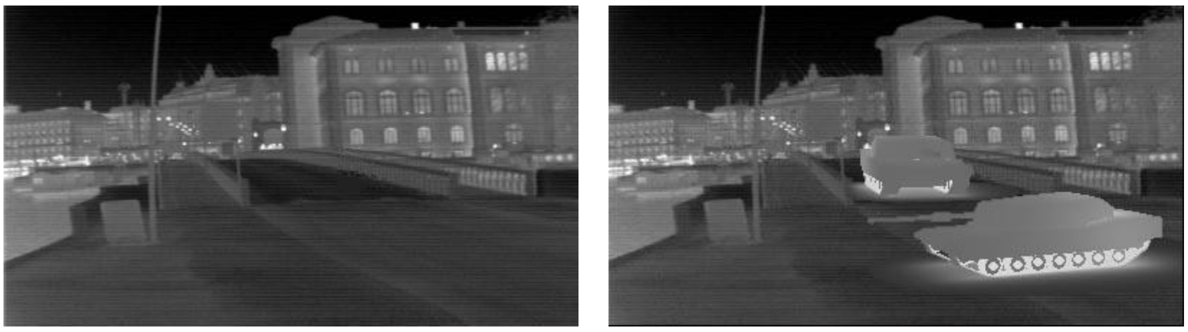
Figure 2.1 The synthesis procedure of infrared targets and the background [WWBP01].

Molecular Dynamic for Conduction. Molecular dynamic (MD) methods are now generally accepted approaches for simulating molecular scale models of matter. The essence of MD simulation methods is simply stated: numerically solve the N-body problem of classical mechanics. H. Xue and C. Shu [XS99] presented investigation to deals with the equilibration of heat conduction simulation in a very thin film using MD. David M. Harrild et al. [HPH00] described the novel application of a Finite Volume method (FVM) derived from computational fluid dynamics to the field of computational cardiac electrophysiology. They applied this method to simulate conduction in an arbitrarily shaped or complex region. Jiaocheng Ma et al. [MXJ08] proposed real-time mathematical 2D heat transfer and solidification model. This model was presented for billet continuous casting of low carbon steel and solved by FVM. The GPU-based implementation is faster than that of CPU-based MD simulation. Juekuan Yang et al. [YWC07] presented an implementation of MD simulation on modern graphics processing units (GPU). This GPU algorithm was used to calculate the thermal conductivities of solid argon and to reduce the total computational time of conduction simulation at high performance. These methods mentioned above are used to analyze and solve heat flux propagation on a single solid object but they are difficult to represent interaction with other objects.

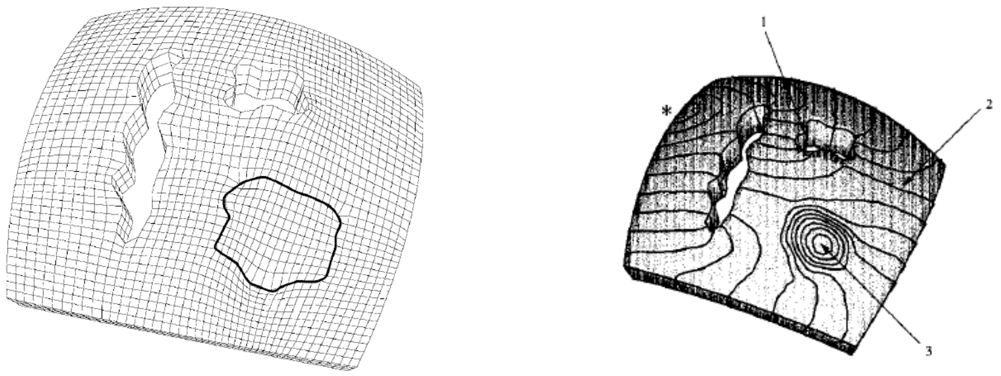

Figure 2.2 The mesh used to incorporate a complex conduction environment and the result of stimulation [HPH00].

Fluid dynamic. The solution to a fluid dynamics problem typically involves calculating various properties of the fluid, such as velocity, pressure, density, and temperature, as functions of space and time. Wei Li et al. [LWK03] presented a physically-based flow simulation which supports complex boundary conditions running on the general-purpose graphics hardware. For computing the flow field, they accelerated the computation of the Lattice Boltzmann Method (LBM) on GPU, by grouping particle packets into 2D textures and mapping the Boltzmann equations completely to the rasterization and frame buffer operations. To handle complex, moving and deformable boundaries, they proposed a generic voxelization algorithm of the boundaries using depth peeling, and extended it to a dynamic boundary generation method that converts any geometric boundary to LBM boundary nodes on-the-fly. Zhe Fan et al. [FKZQ*09] presented a simulation and visualization system for the thermal fluid dynamics inside a pressurized water reactor of a nuclear power plant when cold water is injected into the reactor vessel. They employed a hybrid thermal lattice Boltzmann method, which has the advantages of ease of parallelization and ease of handling complex simulation boundaries.

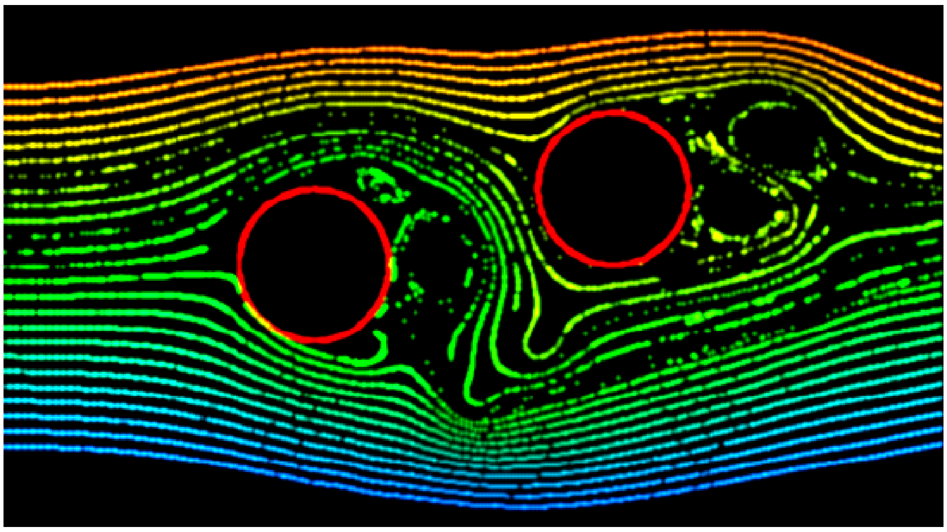
Figure 2.3 Particles advected in a 2D flow field based on the D2Q9 LBM model [LWK03].

3. Overview

In this chapter, we will briefly describe our method and each chapter afterward.

We propose our voxelization algorithm in chapter 4. The energy of molecules on object surface may not be the same in dynamic state of heat transfer. The objects in simulation should be divided into voxels as tiny as well. We generate voxelized textures from objects by depth peeling in axis-aligned orthogonal views. These textures which stored energy and geometrical information are able to compute variation of heat in parallel through GPU. Since the method is only valid to surfaces, we fill the voxels in multiple layered textures with large weight of heat capacity for simulating volume of object. By comparing with full volume resolution, our methods compress voxel number into 10~25%.

Chapter 5 includes the details of heat transfer simulating. In order to rapidly generate visually reasonable scene in simulation of radiation, we ignore the interactive reflection between objects with low temperature difference. We implement shadow map and Phong shading model while low intensity heat source. In addition, screen space ambient occlusion (SSAO) [Mitt07, RGS09] is used to enhance detail in high temperature difference.

To simulate conduction, we separate the render pass into pruning, contact detection and spreading phases. First, we use the linear-time CULLIDE [GRLM03] algorithm to prune collision-free objects in image space which are unnecessary for computation of heat exchange. Once a collision is detected, the contact surfaces make heat pass through from hot to cool side. We apply Layered Depth Images (LDI) extended method [FBAF08] which processes contacts between objects bounded by triangular surfaces. The last step is spreading. Each object spreads heat through itself until the distribution of heat is equilibrium.

Computation with computational fluid dynamics (CFD) usually involves intensive computation in general convection processing. Due to our real-time and visually acceptable requirement, we represent the shape of object by combination of cylinders. Heat transfer between fluid and such simple shape can get approximate distribution [BJO98, KCY06]. By appling this approximation we can speed up the calculation between surface and fluid from O(n^3) to O($n^2 logn$) which n defined boundary of the scene.

Our experiment and result are presented in chapter 6. According to performance and visual result, we provide optimal parameters for this simulation system. At last, we summarize our approach and discussion in chapter 7.

4. Voxelization of 3D Model

Since the temperatures between various parts of an object may not be the same, we should divide the object into regular volumes, so called voxels, with its own thermal energy for simulating heat transfer in dynamic state. A voxel is a volume element, comprising a value on the regular grid in three dimensional space. In our system, the variations of temperatures on object surfaces are displayed by voxels in continuous domain.

4.1 GPU-Based Voxelization

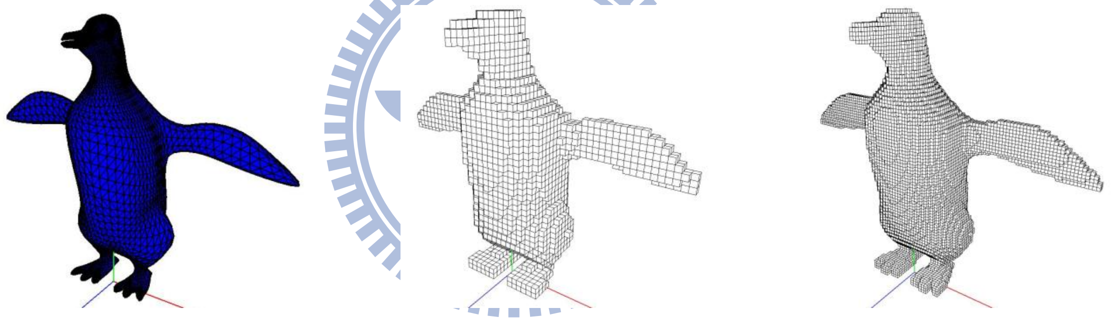

Figure 4.1 From left to right: mesh of penguin, large voxel size and small voxel size voxelized model by slice method. The smaller voxel size results more precise shape of mesh and more storage data used.

An intuitive voxelization approach is the slicing method [FC00]. This method sets distance of near and far clips planes as a single voxel size and renders only the geometry falling into the slab between the two clip planes. The clip planes are shifted to generate subsequent slices until entire volume covered with these slices. Our simulation method mostly interacts around surfaces of objects which are sparse in a volume slice in most case. In other words, only a small percentage of voxels are intersected by the boundary surfaces. There is no need to voxelize the empty space that corresponds to non-boundary voxels. Furthermore, only self heat spreading involves interior volume and we present how we reduce the amount of voxel and keep visually-similar approximation in chapter 4.3.

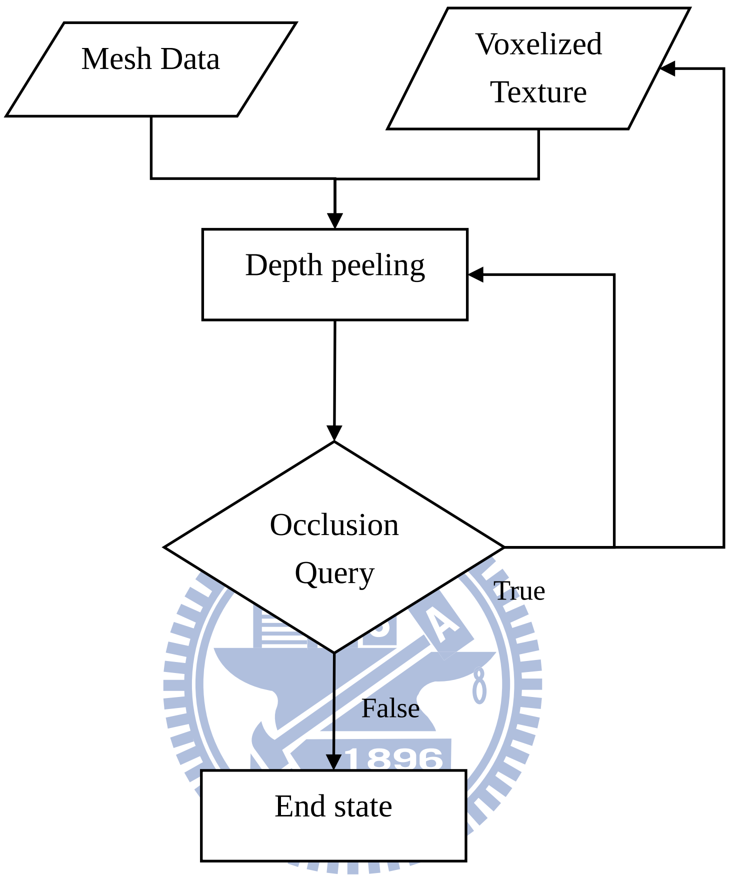

Figure 4.2 The flow chart of GPU-based voxelization algorithm.

The GPU-based voxelization algorithm we used is the method proposed by Wei Li et al. [LFWK03]. They avoid a slicing method by the idea of depth peeling [Ever01] used for order-independent transparency. The depth layers in the scene are stripped away with successive rendering passes. The procedure can be divided into three steps:

1. At first, the scene is rendered normally and the layer of nearest fragments as voxels is obtained. During the second rendering pass, each fragment compares depth value with the depth texture obtained from the depth buffer of the previous pass.

2. The fragment is discarded if either depth test is not pass or depth value greater than that depth texture.
3. The process continues until no fragment is farther away than the corresponding pixel in the depth texture. This condition is best determined by using a hardware occlusion query, which returns the number of pixels written to the frame buffer.

We apply the peeling process three times. Each time, the image plane is orthogonal to one of the major axes. The viewport is translated so that the layer images do not missing voxels but are tiled as tightly as possible.

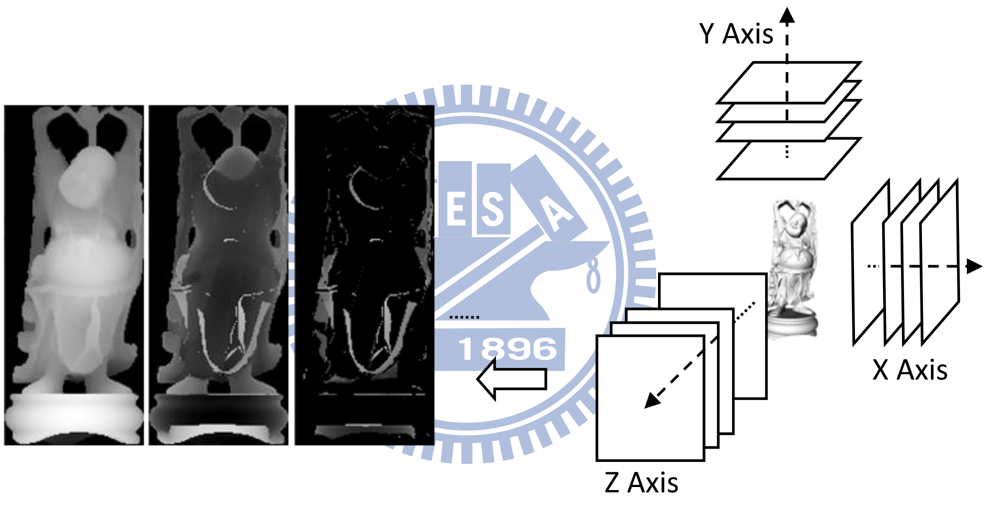

Figure 4. 3 Voxelized textures of “Happy Buddha”. There are 18 layers in x axis, 20 in y and 8 in z; the left shows depth value in the first three textures of z axis.

We apply depth peeling and save layer images with depth value in textures named voxelized texture. There are three series of voxel data from each orthogonal view in these textures as shown in Figure 4.3. The 3D position of voxel can be restored as texture coordinate and depth in voxelized texture. As a result of peeling from three orthogonal views, some of the voxels may be rendered more than once. The replication does not affect the accuracy but we can reduce it to save more space and computing times.

4.2 Optimization of Voxelized Texture

We get voxelized textures by three-view depth peeling algorithm but these voxelized texture data can further be optimized for acceleration of simulation system.

The improvement mainly occurs at overlapping areas in voxelized textures if the areas can be rendered from two or three orthogonal views. We take a sphere for example. Figure 4.4 shows the first voxelized textures from x and z axis. These textures which are rendered as hemisphere of the sphere overlap at the same quarter with another one. Though all voxels are unique in single orthogonal view, the same area may be rendered repeatedly by each peeling process in the worst case. That means we may simulate on the same voxel twice or more but it is not necessary. Therefore, we should store each voxel only once in all voxelized textures.

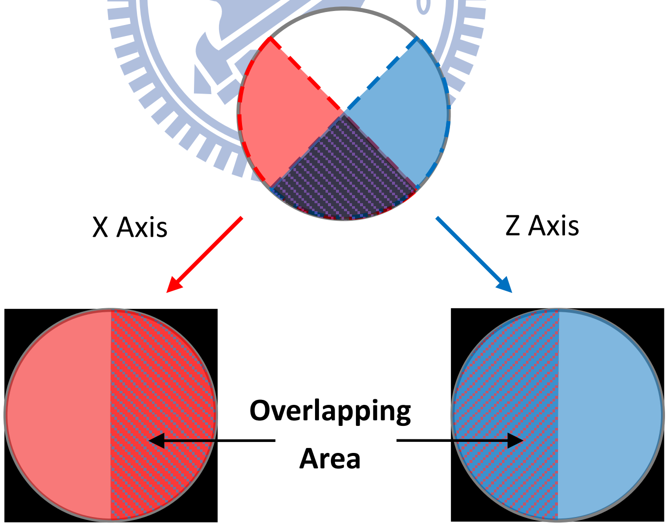

Figure 4.4 The first layer images from orthogonal view on X and Z axis overlap on cross area.

To keep the structure of voxel integrity, stored areas in each axis-aligned texture must be independent of other orthogonal views. Then, we consider the attribute of surface normal to check each fragment on voxelized texture whether the absolute normal weight of view axis is greater than other two axes. For instance, if *n* is normal vector of surface and absolute normal weight of x-axis $\| n_x \|$ is greater than $\| n_y \|$ and $\| n_z \|$, the corresponding fragment is preserved as a voxel in x-axis peeling process.

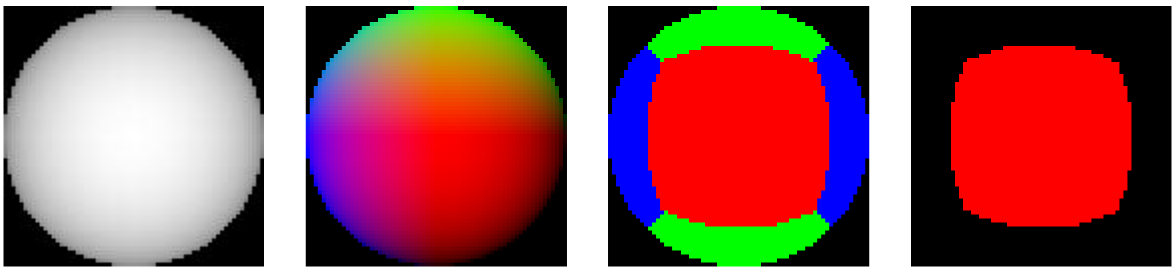

Figure 4.5 Voxelized texture of sphere rendered from x axis: (a) depth value; (b) normal of surface; (c) repainting red on fragment if $\| n_x \|$ is greatest, green for y axis and blue for z; (d) preserved area of (c).

After removing replication of voxelized textures, more empty space may be generated due to image space quantization at view change. As shown in Figure 4.6 (a) and (b), some of these textures contain only few voxels or completely empty. We pack texels to fill empty space before its texture as forward as possible and remove textures without any voxel data. Through packing textures process, the number of layers is decreased which affects the number of simulation computing times. We compare the textures of “Happy Buddha” with/without data packing. The number of layers decreases to a half.

The last step of optimization is to build connection of voxels. We do not know whether these voxels connect others around after packing. Even though we can find the connection by restored 3D position of voxels, it has to be precomputed to reduce traversal neighbor texels every time.

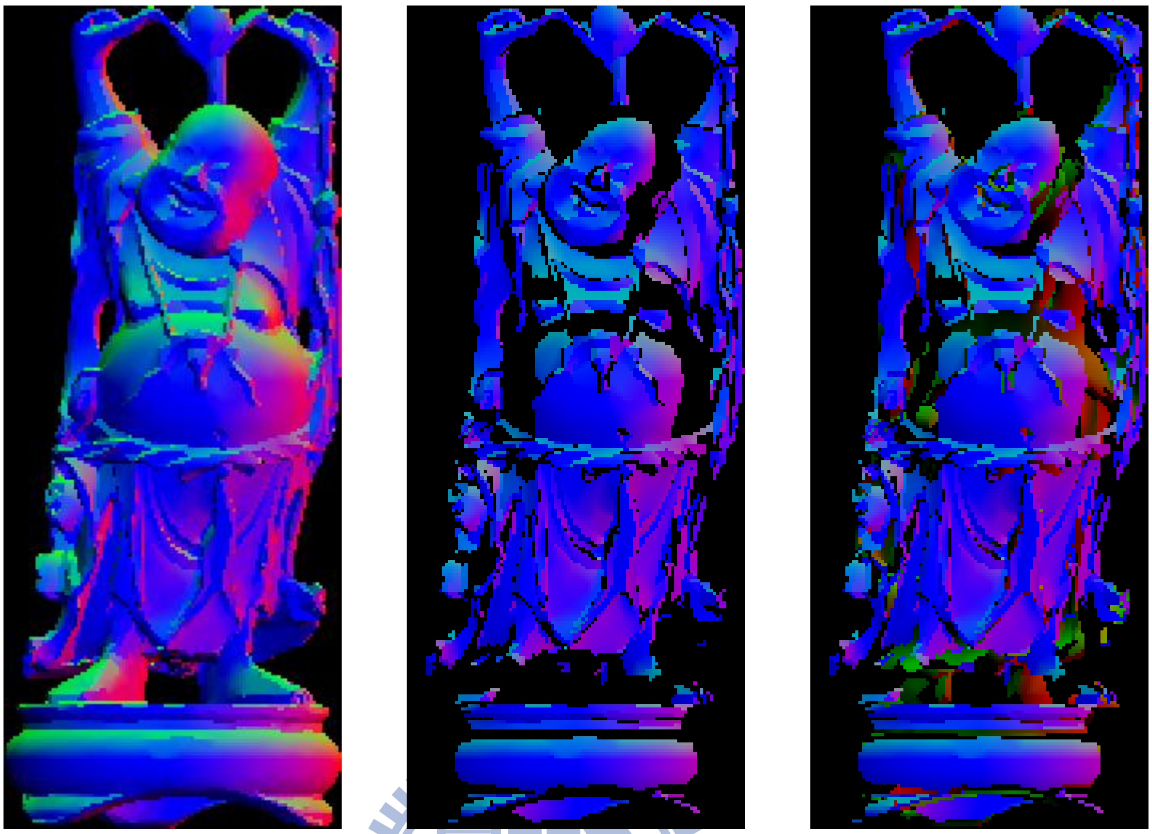

(a) **(b)** **(c)**

Figure 4 6 Voxelized texture of "Happy Buddha" rendered from z axis with surface normal, from left to right: (a) original, (b) stored and (c) packed texture. After packing, the number of layers in x is 8, 11 in y and 6 in z axis.

We summarize the procedure of optimizing voxelized textures. First we remove the replicate voxels by comparing absolute normal weight of orthogonal axis. The voxels with maximum absolute normal weight in viewing axis should be preserved. We pack the preserved voxels as forward as possible in voxelized textures for fill the empty spaces. After packing, we reduce the layer if layer of texture is completely empty. At last step we reconstruct the connection of voxels and save connecting information in corresponding textures. Figure 4.7 represents the sample of optimizing procedure.

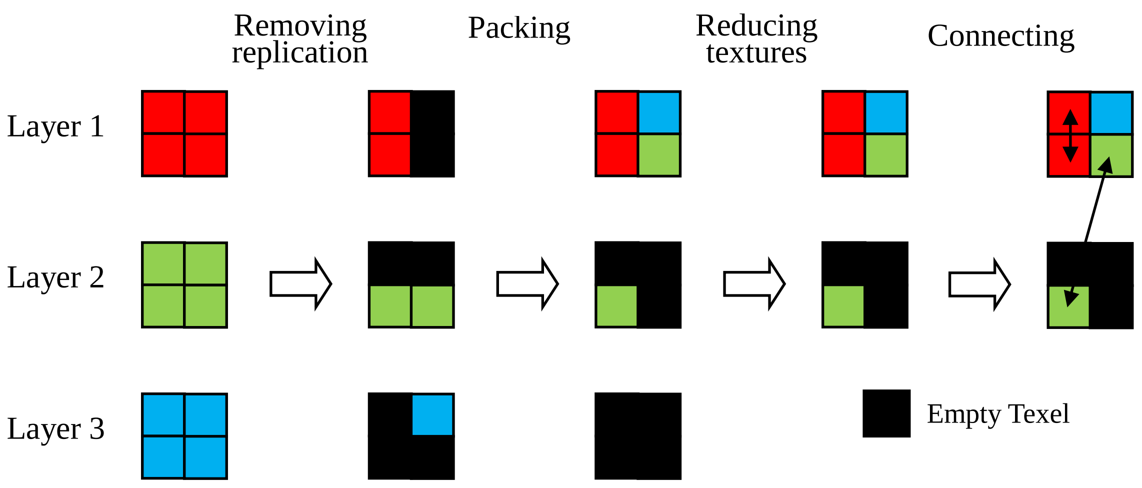

Figure 4.7 The example of optimization of voxelized texture.

4.3 Multi-Level Voxelized Texture

Our voxelization algorithm generates only a single shell of target model. However, not all of objects fit in this case; it may be solid or more complicated structure inside. We will deal with solid and uniform material for conduction simulating. For this reason, we build voxelized textures inside the shell.

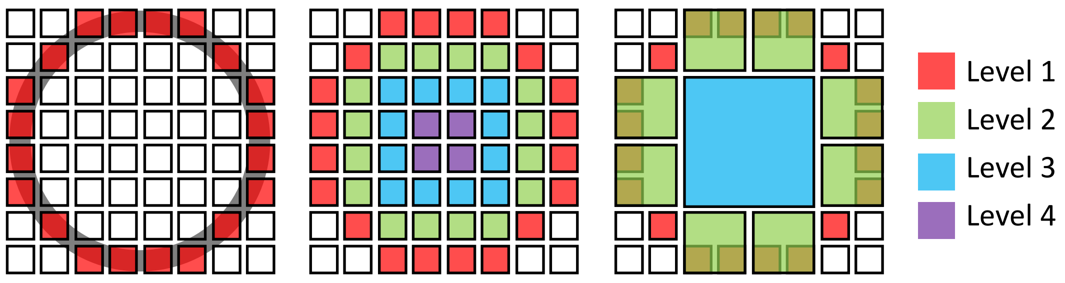

Figure 4.8 Voxelized texture of sphere slice. From left to right is single shell, multi-level and irregular multi-level. The irregular multi-level varies voxel size with different levels. Because of overlap occurring on some voxels, the conduction weight between voxels should be adjusted.

We can build inner textures easily from original object and shell textures. If we construct all voxels inside of object with the same size of shell voxels, the number of textures explosively increases and it cannot take our advantage of acceleration anymore. The voxels inside should be considered with larger capacity than those outside, and then we only need to build fewer textures for interior voxels.

We use a half resolution to record interior voxel data. Such as mipmap texture, each level means one more layer inside and texture size smaller than level before. Figure 4.8 shows the voxelized texture of sphere slice by single shell, multi-level and irregular multi-level. The voxel size is presented as conduction weight between different levels of textures in simulation. Besides, we must be careful about increasing voxel size, and total capacity must be kept in original volume. We discuss multi-level and irregular multi-level structure in chapter 5 and 6 in detail.

We construct multi-level structure on full volume voxel data but our voxelized texture. Since adding one level means to add the same size of our voxelized texture, it is difficult to divide a large amount of voxels inside into three axis-aligned textures. However, we can build the irregular multi-level structure in voxelized texture. There are few irregular voxels inside because of the voxel size increasing exponentially each level.

5. Simulation of Heat Transfer

5.1 Radiation from Heat Source

According to Stefan–Boltzmann law, the power emitted per unit area of the surface of a black body is directly proportional to the fourth power of its absolute temperature. That is

$$q'' = \sigma \varepsilon T^4 \tag{1}$$

Where *q''* is the total power radiated per unit area, *T* is the temperature in the Kelvin scale, ε is the thermal emissivity and $\sigma = 5.67\times10^{-8} \mathrm{W \cdot m^{-2} \cdot K^{-4}}$ is the Stefan–Boltzmann constant. It means that anything emits thermal radiation if it is higher than absolute zero in temperature. Besides, thermal radiation may be absorbed, reflected or transmitted. It is difficult to apply radiosity algorithm with each feature in real-time. For the reason, we approximate parts of processes of total radiation and simulation with the following assumptions.

At first, the heat source, such as the sun, emits thermal energy to the scene. In general case, the environment temperature is about 300K and the sun is about 5800K. During the daytime, the sun emit energy about $1000\mathrm{W \cdot m^{-2}}$ to Earth. In contract, the energy emits from other object can usually be omitted because of low temperature difference. We assume the max temperature difference in the scene to be 100K, if there is no additional heat source, and the max radiation is about $31.15\mathrm{W \cdot m^{-2}}$(distance between objects: 10m). We project this energy to cubes with different materials whose volume is $1\mathrm{m}^3$ and assume cubes absorbing energy fully as black body. The variations of temperature are shown as Table 5.1. Actually, these materials cannot completely absorb the energy and the variations of temperature may be close to zero.

As this result, we only calculate radiation from heat source to the scene but from other objects.

Table 5.1 The variations of temperature by fully absorbing 31.15Wm^{-2} on 1m^3 cube.

Material	Density **kg/m^3**	Heat Capacity(25℃) **J/(kg·K)**	ΔT **K·s^{-1}**
Platinum	21.45×10^3	135	1.08×10^{-5}
Gold	19.3×10^3	126	1.28×10^{-5}
Mercury	13.58×10^3	140	1.64×10^{-5}
Lead	11.34×10^3	128	2.15×10^{-5}
Silver	10.49×10^3	233	1.27×10^{-5}
Copper	8.96×10^3	386	9.01×10^{-6}
Iron	7.87×10^3	444	8.91×10^{-6}
Diamond	3.5×10^3	509.1	1.75×10^{-5}
Aluminum	2.7×10^3	897	1.29×10^{-5}
Water	1×10^3	4186	7.44×10^{-6}
Alcohol	0.79×10^3	2440	1.62×10^{-5}
Gasoline	0.73×10^3	2220	1.92×10^{-5}

Since the reflection term is based on intensity of heat source but variation of temperature, it cannot simplify as emission. At assumption of the radiation under a single wavelength, objects between A_i and A_j, the intensity of radiation from patch dA_i to dA_j is:

$$dq_{i\to j} = I_i \cos\theta_i \, dA_i \frac{dA_j \cos\theta_j}{R_{ij}^2} \tag{2}$$

I_i is the intensity of A_i, θ_i andθ_j is included angles between $\overline{dA_i dA_j}$ and normal of patches and R_{ij} is length between dA_i and dA_j. If the distance is too far from heat source to object surface or heat source is very small as a point, such as the sun, the intensity of radiation can be formed as the diffuse term in Phong reflection model.

$$I_d = k_d(L \cdot N)i_d \tag{3}$$

k_d is diffuse reflection constant, L is the direction vector from the point on the surface toward each light source, N is the normal at this point on the surface and i_d is intensity of light source. The ambient term in Phong model is to simulate accumulated inter-reflection in the scene but it is unidirectional and too rough for complicated scene. The reflection of radiation is similar with global illumination which contains direct and indirect light computing. We can get the first reflection from heat source easily but it's costly to compute indirect reflection repeatedly until thermal equilibrium. For simulating dynamic scene in real-time, we use Phong model and shadow map to render direct light and ambient occlusion map to approximate indirect light if the scene is complicated.

We assume that all materials in the scene are opacity to simplify the problem. For these assumptions, we only deal with emission and reflection of radiation from heat source as the scene by using Phong model and shadow map, optional indirect reflection by ambient occlusion if the scene is complicated. We render the emission of heat source to voxelized textures represented each object in the scene. The reflection is rendered in screen independently and blended with final results.

5.2 Heat Propagation

The area irradiated by heat source gains energy and the heat is propagated in the whole solid object until energy balance. In each rendering pass, we spread the energy of voxels to connected neighbor for each voxelized texture.

$$q = k \cdot \frac{A}{L} \Delta T \tag{4}$$

In conduction equation (4), k is the thermal conductivity of material, ΔT is variation of temperature, A is contact area and L is the distance between two elements. For a single object, we can get A, L and ΔT from voxelized texture and set the same k for all voxels.

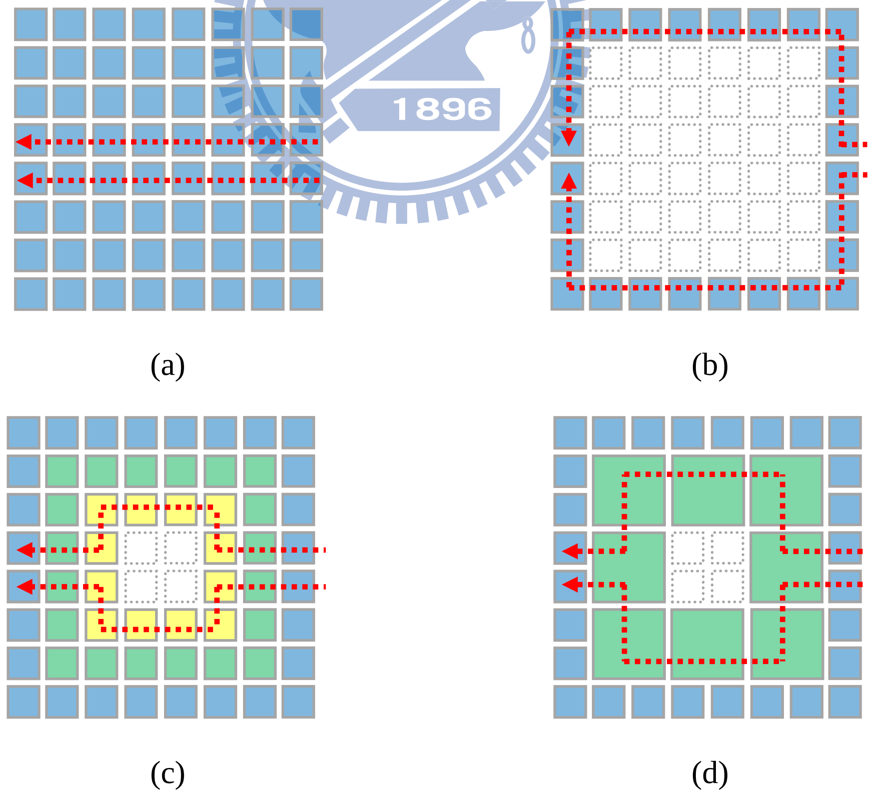

Figure 5.1 Four styles of voxelization: (a) full volume, (b) single shell, (c) multi-level and (d) irregular multi-level. Red lines are shown the shortest heat flux paths form right to left side.

As we mentioned in chapter 4.3 for efficiency, we do not build regular voxels but multi-layer voxelized texture for an object instead. By comparing the different voxelized structures as shown in Figure 5.1, the shortest path shown as a red line in Figure 5.1.(b) only is through the shell voxels and cause the difference of propagated result. Figure 5.1.(c) shows multi-level as inside voxels. Although it may not have exactly the same result of propagation, it could be approximation as Figure 5.1.(a) with close number of voxels. Figure 5.1.(d) shows less voxels than (c) but different size of voxel between shells. Since the size of voxel is varying with different levels, *k* should be increased with the size.

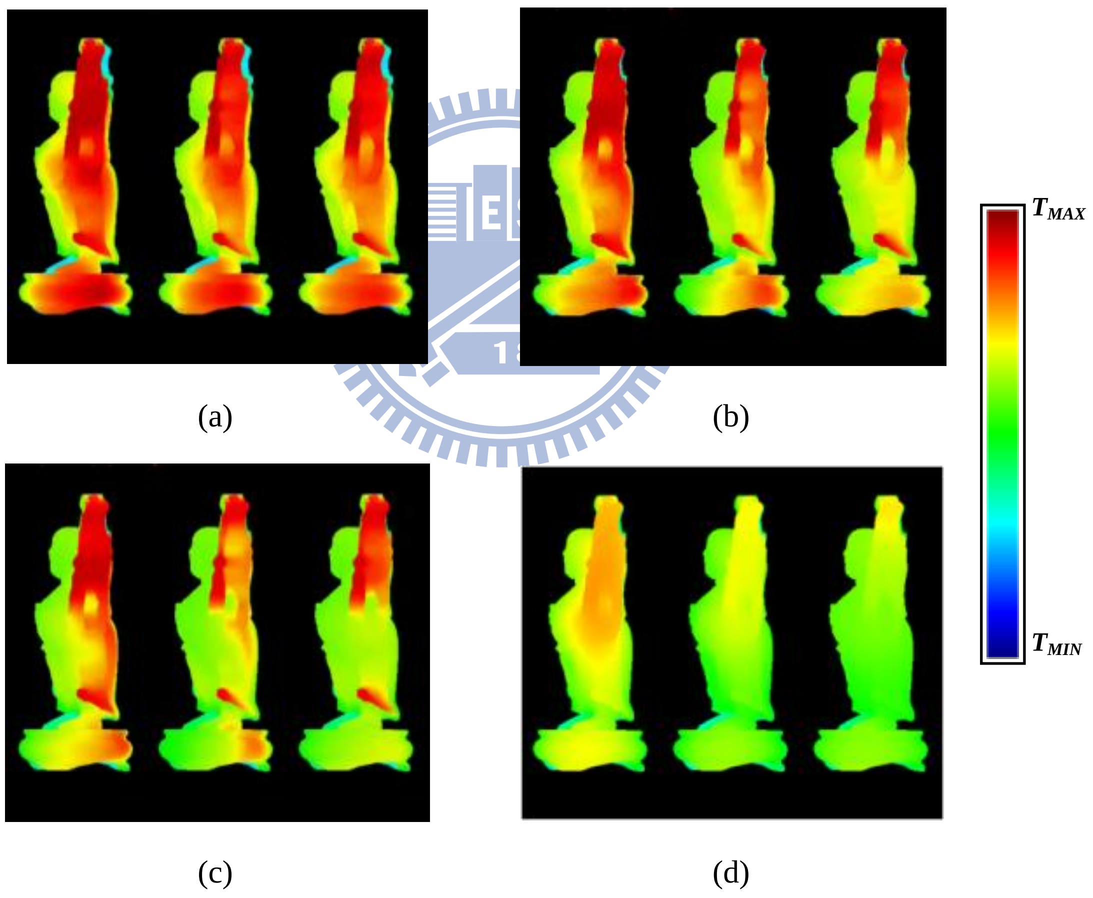

Figure 5.2 Heat propagation of “Happy Buddha” from left to right are single shell, multi-level and full volume, with each time steps: (a) 30s, (b) 60s, (c) 90s and (d) 180s.

It provides that the average heat energy is close to standard case shown as Figure 5.1.(a) in thermal equilibrium by filling the same volume size inside. The dynamic states may appear artificially as shown in Figure 5.2. The variation of middle one in Figure 5.2, which is irregular multi-level, is a approximation with right hand side, which is full volume, but still distinct in detail. We need to adjust the weight of conduction for acquiring the result as real as possible.

5.3 Conduction by Contact

We propose approximation of conduction on a single solid object in section 5.2. However, it cannot perform conduction between two objects directly. All of we known is the connection of voxels in each indivisual object and it is not enough to realize whether there're contacts between two objects in dynamic. We can apply conventional collision detection between objects but it results in intensive computation for objects with considerable voxels. Because conduction only occurs around contact surface of objects, we take advantage of voxelized texture and compute only the voxels in the most exterior shell as surface. These voxelized textures can be used by image-based collision detection method [FBAF08] which processes contacts between objects by GPU acceleration. We only compute the interaction areas of surfaces where the heat conduction exactly occurs.

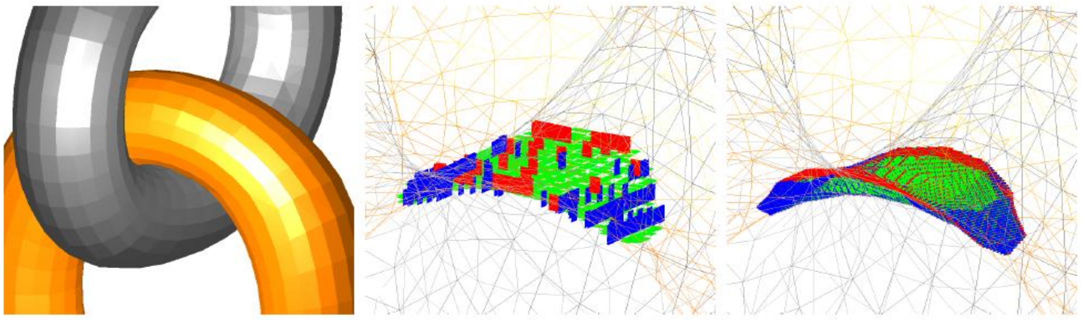
Figure 5.3 Intersection volume at different resolutions. Left: the collision surfaces. Middle: the intersection volume at resolution 16×16. Red, green and blue pixel show the bounds in x,y and z directions, respectively. Right: resolution 256×256. [FBAF08]

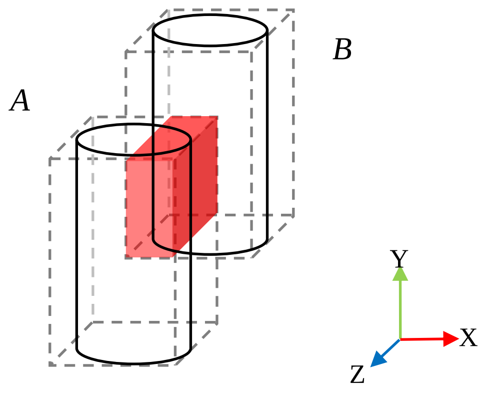

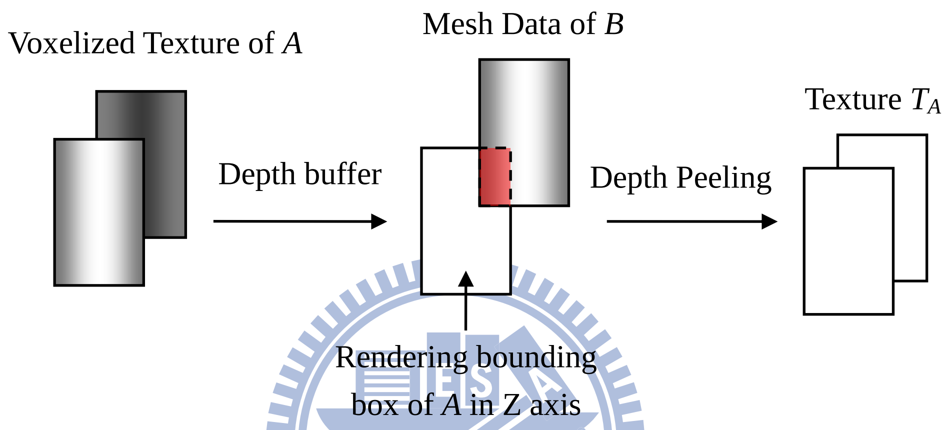

Figure 5.4 The example of two cylinders contact. We render *B* on bounding box of *A* in Z axis and apply depth peeling. Voxelized texture of *A* replaces depth buffer in peeling process. The texture T_A records contact area on surface of *A*.

At each time step, our algorithm performs the following steps:

- Find pairs of objects with overlapping bounding boxes (broad phase).
- For each pair of objects *A* and *B* with overlapping bounding boxes:
  1. Set the rendered volume as the bounding box of *A* and render the mesh *B* by GPU.
  2. For each voxelized texture of *A*, compare the depth of *B* with depth value of voxelized texture as depth peeling. If the two depth values are close within a threshold, render this fragment to texture T_A; otherwise, discard the data.
  3. If there is no more fragment of *B* can be rendered or loop of step 2 finishes, exchange *A* and *B* then repeat step 1 and 2 again.

4. If the texel of T_A is stored voxel energy of *B*, perform the conduction with voxelized texture of *A* and the same as T_B and voxelized texture of *B*

In broad phase, we can use CULLIDE algorithm [GRLM03] to check overlap of objects in an image-space method. It provides more precise results than those by computing overlap of bounding boxes. The step 1 to 3 is similar to the depth peeling method we used before. The only difference is depth test between two objects *A* and *B*. In step 3, occlusion query can be applied as well. This algorithm does not perform physical collision but it can be alternative and easily to combine with our method.

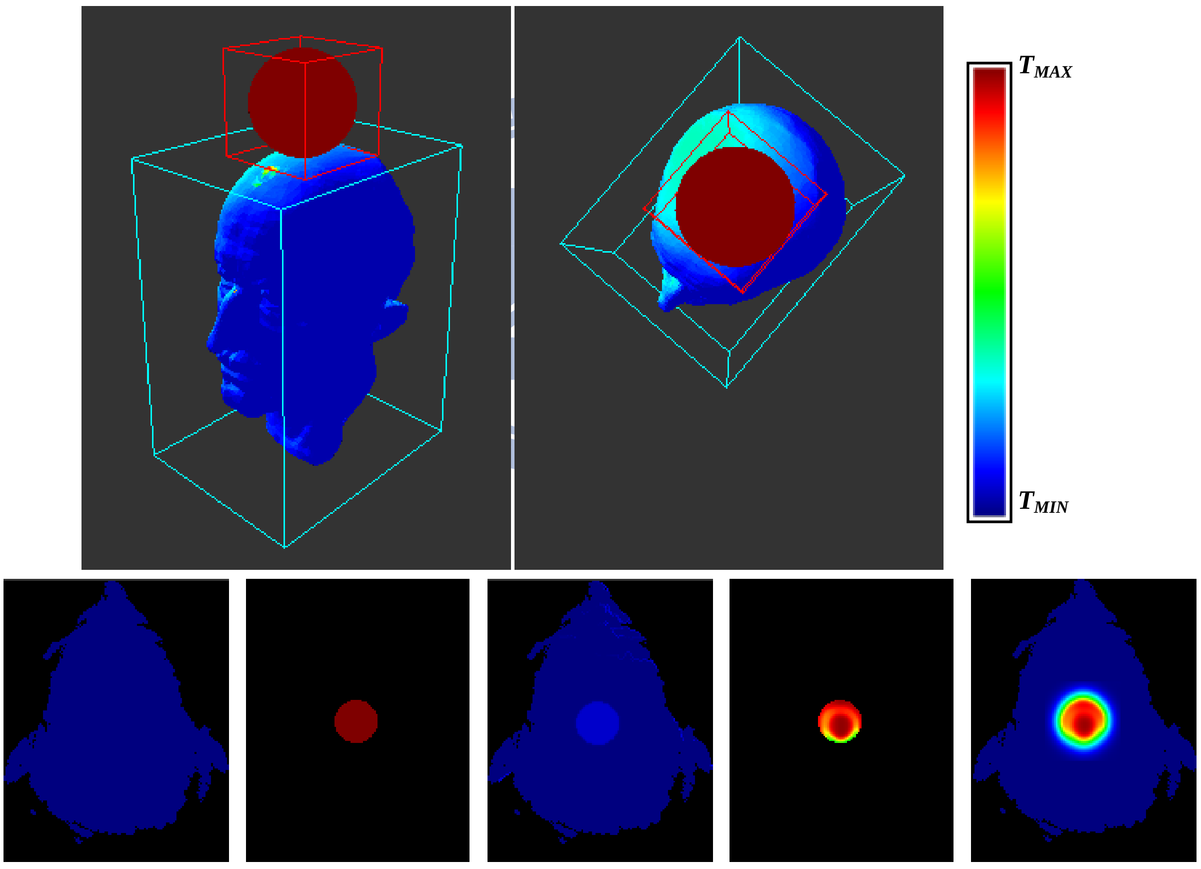

Figure 5.5 The contact of a hat ball and cool Planck's head. The collision area occurs on top of head which is corresponding voxelized texture (a). (b) shows the conduction texture T_{Head}, which records energy of ball at contact. This energy conducts to (a) immediately and heat voxelized texture as (c) shown. The bottom of ball and the top of head conduct and spread the heat after 2 second, and we get the conduction texture T_{Head} as (d), voxelized texture as (e).

We apply image-based collision detection to find contact area to perform conduction between two objects. As shown as Figure 5.5, this process repeatedly until there is no contact of two objects. Figure 5.5 (d) and (e) shows conduction by contact and self-spreading after 2 second in simulation. With these methods, we can simulate fully heat conduction in dynamic scenes.

5.4 Convection in Cylinder Case

One of our goals is to simulate heat convection by wind. In general, particle systems and potential field are used to solve flowing simulation. However, the boundary condition changes dynamic scene and causes difficult computation. We propose computing heat transfer through circular cylinder approximation in cross-flow instead of simulating completely convection.

$$q'' = h(T_s - T_\infty) \tag{5}$$

Equation 5 represents heat convection between surface temperature T_s and environment temperature T_∞, and h is convective heat transfer coefficient. Since it is important to acquire convective interaction with wind speed and local surface, we consider two dimensionless numbers for given flow conditions.

$$Re = V \cdot D / v_T \tag{6}$$

$$Nu_\theta = h_\theta \cdot D / k_f \tag{7}$$

Reynolds number can be defined for a number of different situations where a fluid is in relative motion to a surface. It gives a measure of the ratio of inertial forces to viscous forces. Equation 6 shows Reynolds number definition, where V is speed of fluid, D is characteristic length of object and v_T is the kinematic viscosity varying with temperature. In heat transfer at a boundary (surface) within a fluid, the Nusselt number is the ratio of convective to conductive heat transfer across the boundary. Equation 6 presents Nusselt number definition, where h_θ is convective heat transfer coefficient with angular on circular surface, D is characteristic length and k_f is thermal conductivity of the fluid. We can find the specific curve of Nusselt number in Figure 5.6 by Reynolds number and derive h_θ from equation 7.

$$q_\theta'' = k_f(T_s - T_\infty) \cdot Nu_\theta / D \tag{8}$$

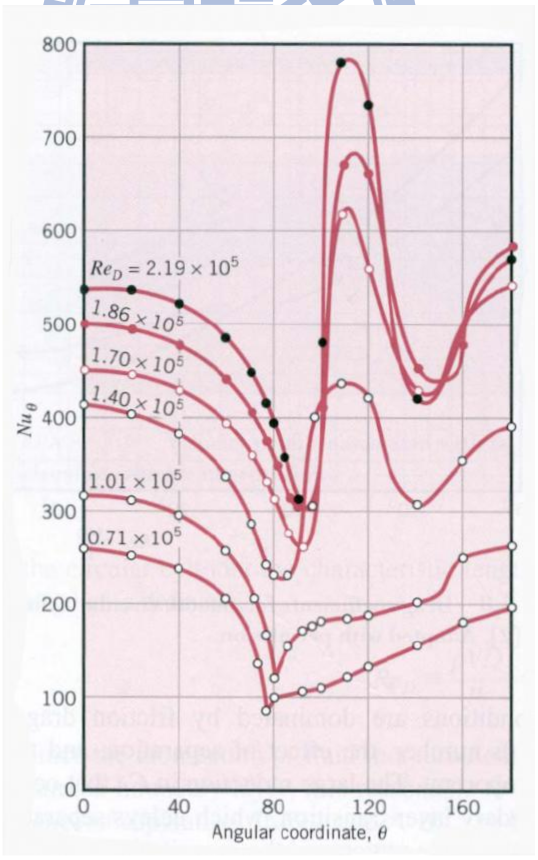

Figure 5.6 Local Nusselt number for airflow normal to a circular cylinder. [IDBL*06]

Equation 8 shows local convection heat transfer in cylinder case where θ is the angle between the surface normal and wind direction. We can project the heat variation from equation 8 to the voxelized texture as surface of object.

This approximation only affects on each single object with laminar flow. It cannot generate turbulent flow to influence the other objects. As shown as Figure 5.7, the wind flow from left to right and a cylinder place in this field. If we place another cylinder behind the present one, the turbulent flow must affects on the second one. However, our method only applies the case of front cylinder on each surface of object no matter where it is.

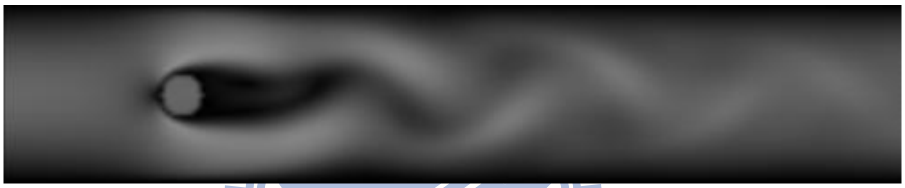
Figure 5.7 The velocity of cross-flow in circular cylinder shows turbulent flow. The dark color represents low velocity, and bright color represents high velocity in flow.

The result of convection is presented in Figure 5.8. The cross-flow streams from left side to right side and cause different variation of temperature with normal.

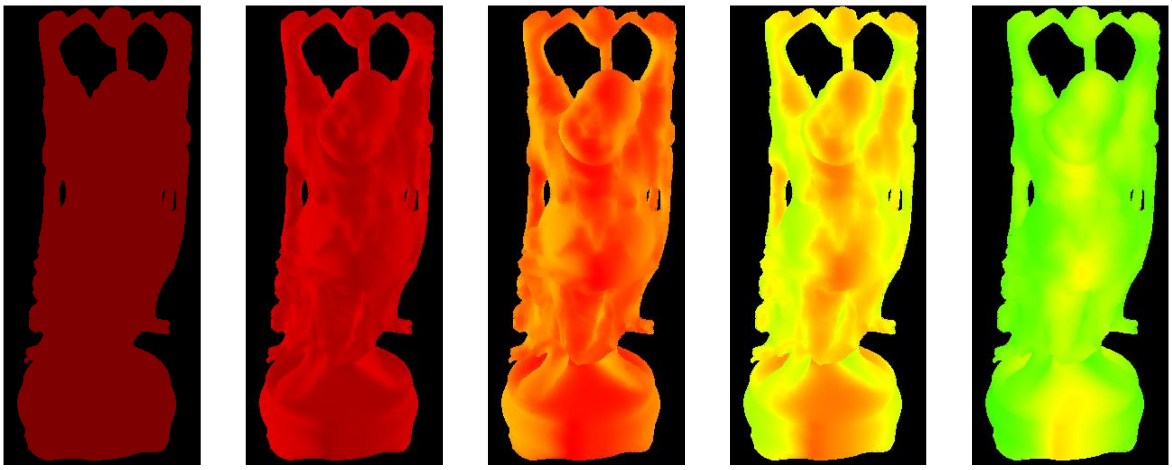
Figure 5.8 The variation of temperature with heat convection as time passes by.

6. Experiment Results

6.1 The Analysis of Voxelized Structure

We introduce several types of voxelized structure, full volume, multi-level, single shell and irregular multi-level. Although these simplified structures could not apply on high-accurate physical analysis, they still provide visually resembling result in simulation of conduction.

The multi-level structure type improves the problem from geodesic distance compared to single shell. The heat passes through from outer shell to interior levels. If the detail parts of object are filled fully by few levels, the variation of heat flux is more precise than single shell. However, it cannot conduct heat as full volume since it remains interior holes in volume. If we use fewer levels for object, it also means more empty space inside the voxelized structure. We cannot fill whole volume of object in multi-level structure type also, or else it forms full volume structure type.

We apply different levels and conduction weights for comparing with full volume structure type. We test single shell, 10 levels, 100 levels and full volume structure type. The result is shown in Figure 6.1. The multi-level type improves the variation as more levels as precise. However, the interior holes influence the variation of whole object. For example, we can observe the sleeves of “Happy Buddha” that show different result between these four cases as time pass by.

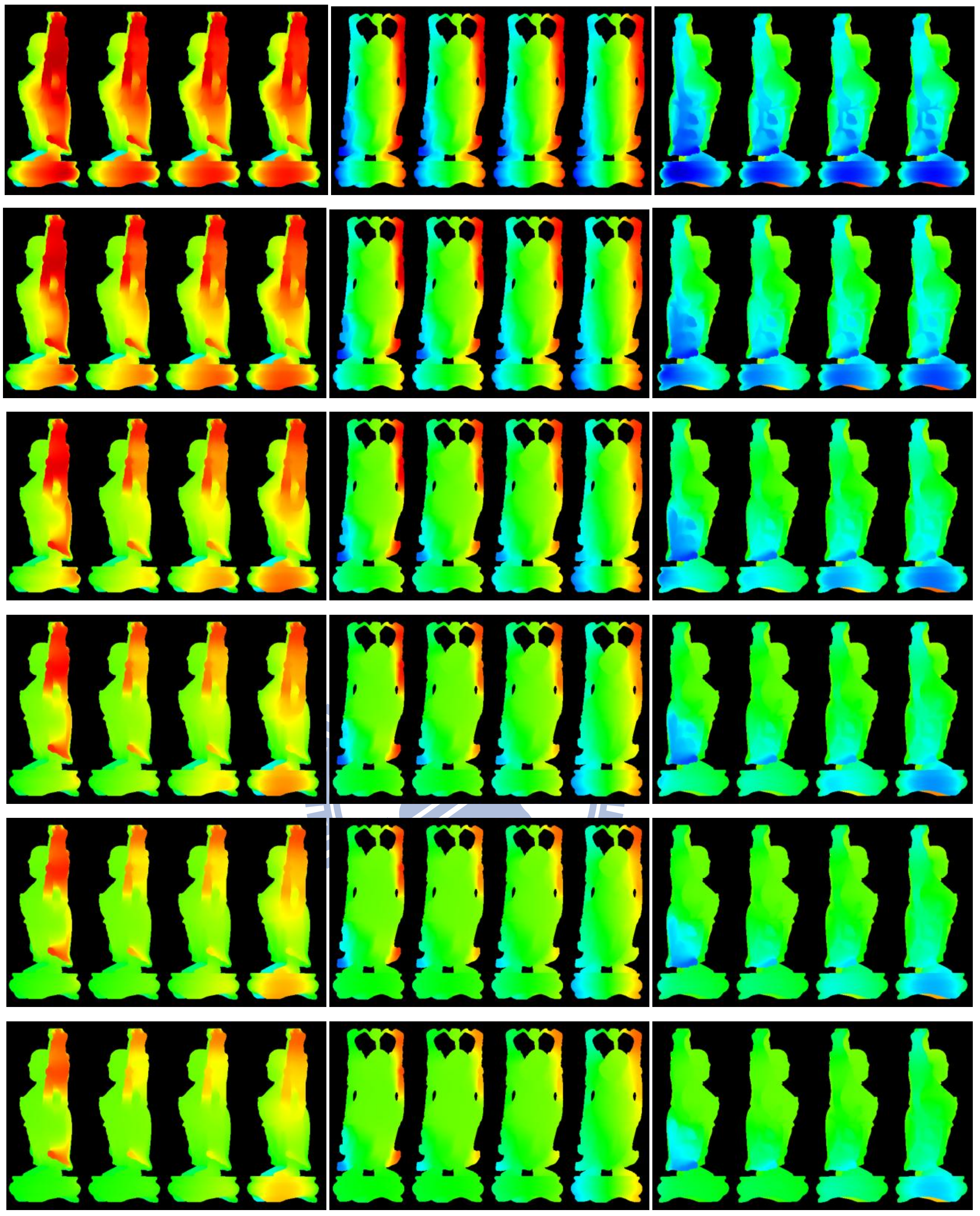

Figure 6.1 The Conduction of "Happy Buddha" with multi-level structure, each row represents the variation of three directions with four different settings through 3600 iterations. There are single shell, 10 levels, 100 levels and full volume structure from the left to the right hand side in a single image.

The irregular multi-level structure type uses different voxel size to fill volume inside. This type may occur overlap or crack between levels because of the complexity of the shape. However, this type contains very fewer voxels against other type. If a cube with side length *n*, there are n^3 voxels in full volume type but $n^2 logn$ voxels in irregular multi-level type. By comparing with regular multi-level type, it is almost fill inside of object with exponentially increasing voxel size. That mean we don't have to consider lot of empty space and whether the heat capacity sufficient or not.

There are 7 levels copied from upper level of reduced size in "Happy Buddha" with 100×250×100 volume resolution. Figure 6.2 shows conduction result comparing with full volume, but an error occurs on s left hand. The error of detail loss appears with overlap and crack. Because of overlap and crack between voxels, we cannot guarantee the heat capacity equal to full volume structure. In other word, the heat capacity in some where occurs overlap or crack may over or not enough.

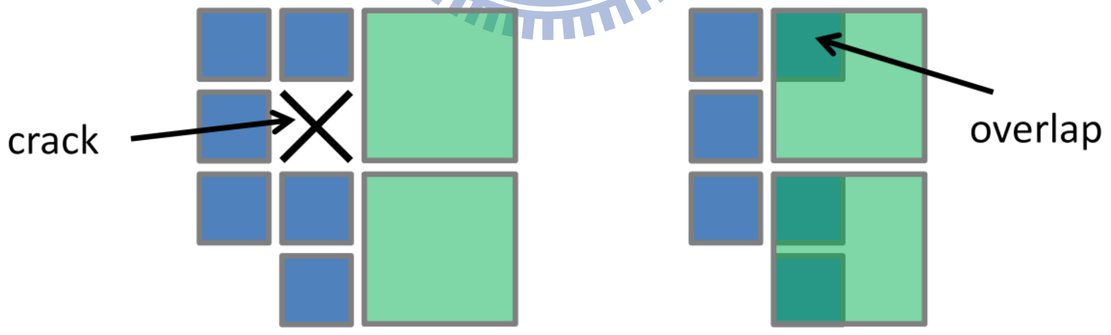

Figure 6.2 The contact area between different levels occur crack or overlap when the model is complex and it samples in high resolution.

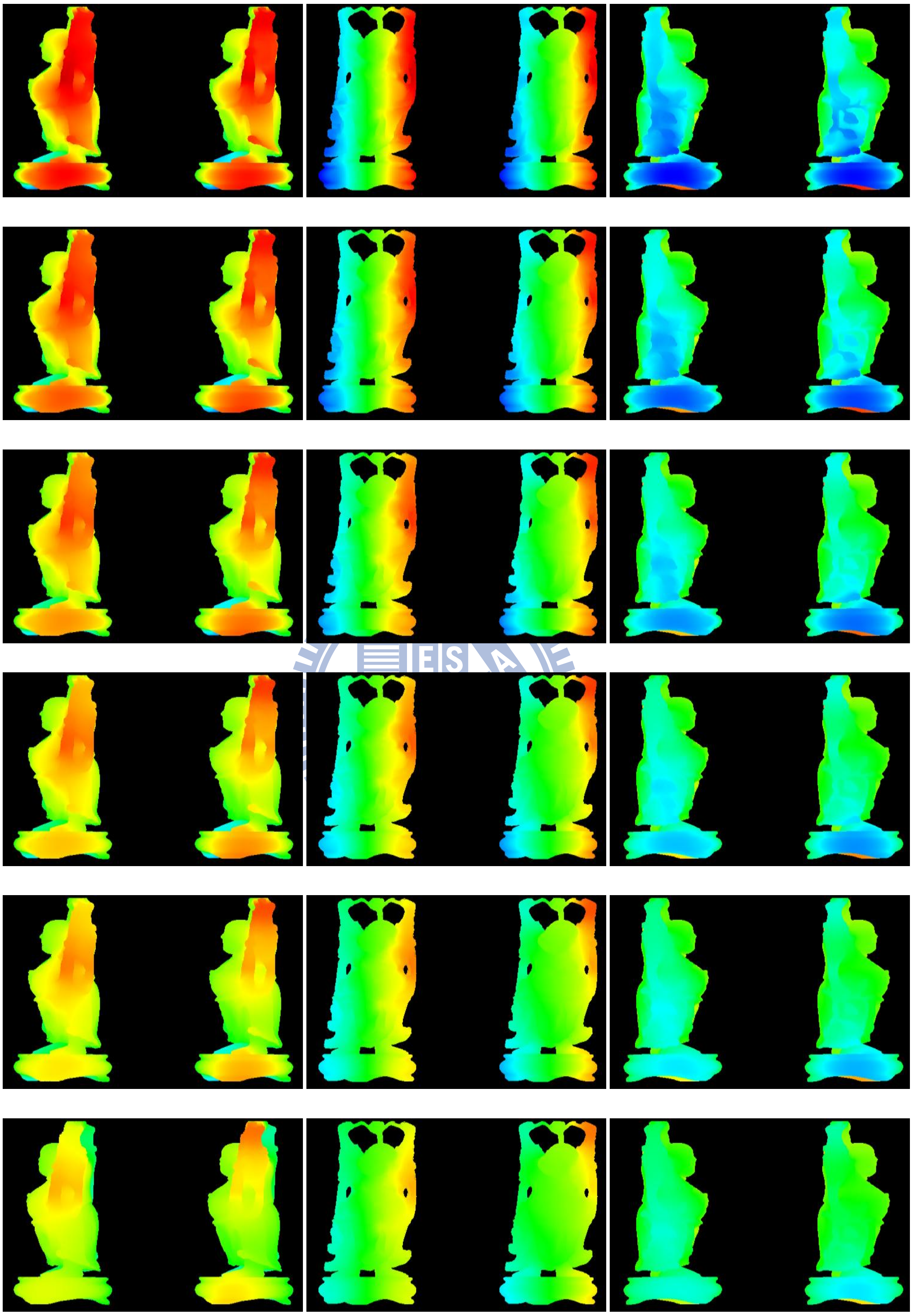

Figure 6.3 The conduction result of irregular multi- level structure and full volume, each row represents the variation of three directions through 4000 iterations.

6.2 Turbulent Flow Effect in Convection

Our convection method in cylinder case cannot generate turbulent flow to influence the other objects behind. We simulate low speed wind flow in a pipe shown as Figure 6.3 by LBM method and calculate average velocity, shown as Figure 6.3 (b) and (d), during the flow fully developed. We can observe from Figure 6.3 (b) and (d), the wind speed only decrease behind the object and form a comet tail. The length of comet tail varies with pipe diameter. The small pipe diameter causes strong pressure and affects flow velocity speedy. In contract, long comet tail appears in the large pipe diameter with weak pressure.

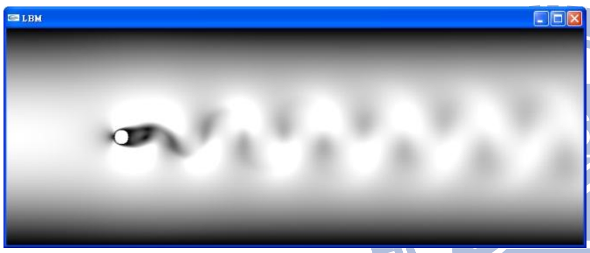

(a)

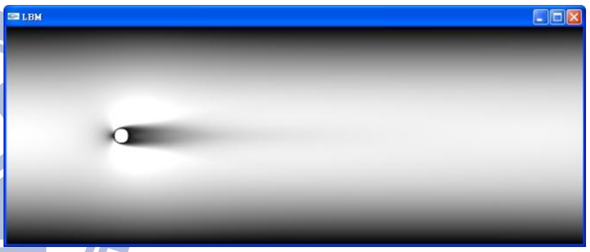

(b)

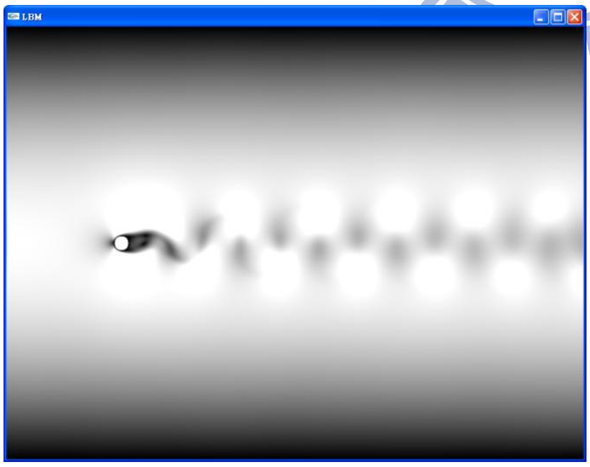

(c)

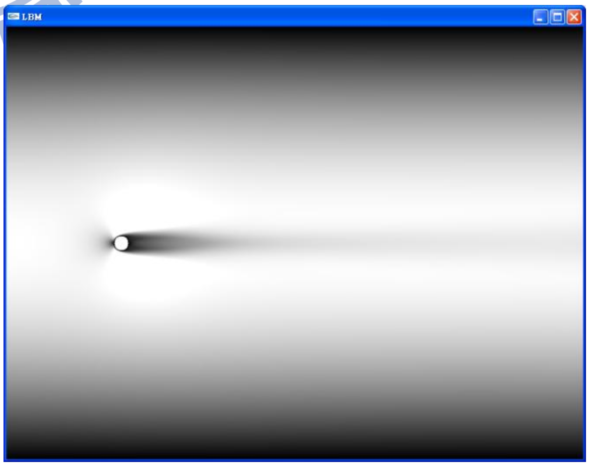

(d)

Figure 6.4 Wind flow simulation by LBM with different pipe diameter 800×300 and 800×600. (a) and (c) show fully developed flow. (b) and (d) show average velocity.

According to the average velocity distribution, we know that the velocity in the comet tail varies from low to high but converging in max speed of wind. We can represent this distribution as a convergent function shown as Figure 6.4. This function provides approximation of turbulent flow effect. If there is an object placed in turbulent flow, we get decreasing velocity from this function and apply convection in cylinder case.

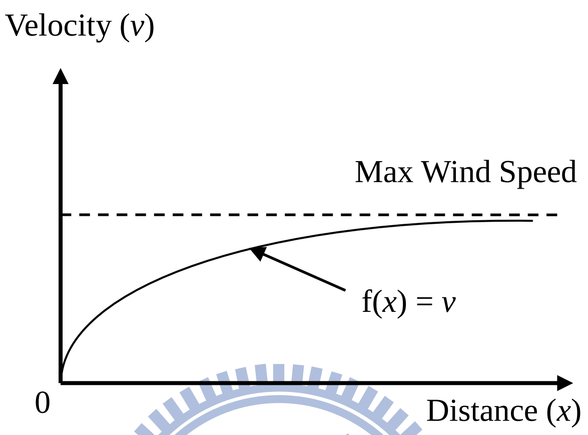

Figure 6.5 The average velocity distribution with distance from the object is represent as a convergent function f(x) = v.

We apply different wind speeds in LBM method with 800×600 resolution and record the varying velocity of comet tails shown as Figure 6.5. In Figure 6.6, we normalized velocity from 0.0 to 1.0 for easy comparing. These curves of normalized velocity are well approximate to the ground-truth simulation and convergence to the maximum wind speed.

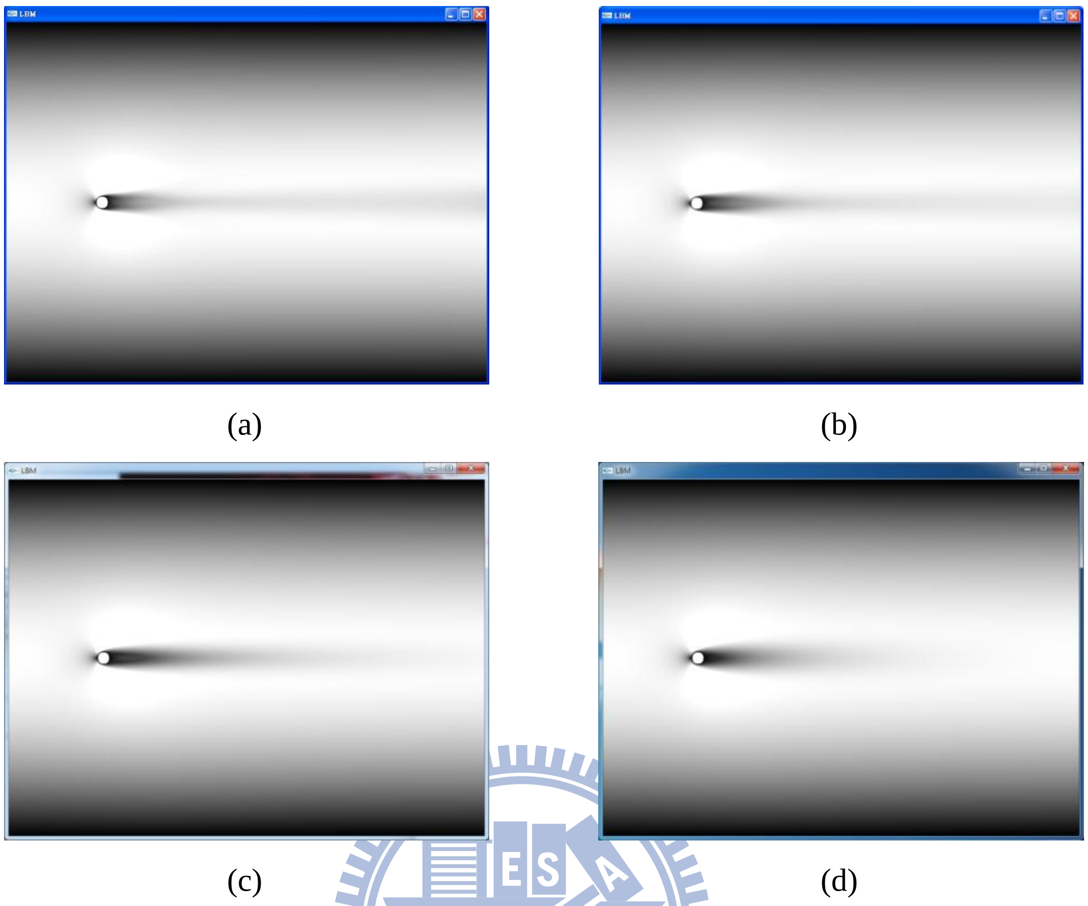

Figure 6.6 The cylinder low by LBM method with different wind speed, (a) 1.0, (b) 0.8, (c) 0.4 and (d) 0.2 m/s.

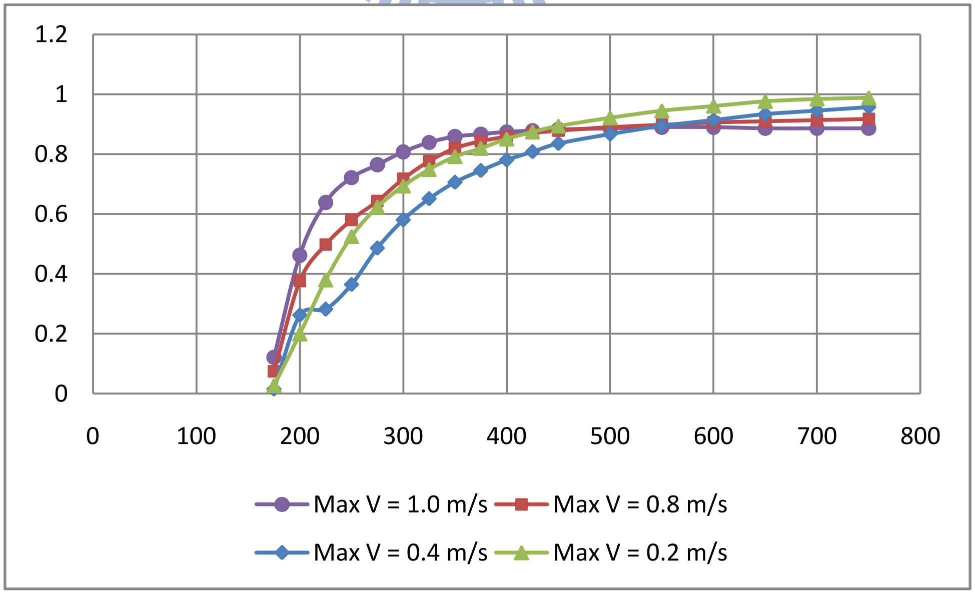

Figure 6.7 The normalized average velocity from Figure 6.3 with distance varying.

6.3 System Performance

Our experiments perform on a desktop with Intel® Core™ 2 Duo E8400 Processor, 3.25GB main memory, and Nvidia 9800GT graphics card. The simulation of radiation and convection only affect on surface of object with rapidly computing. But the process of conduction involves entire voxels in object. The performance of this simulation system mainly depends on voxels of objects in scene. The four types of voxelized structure we mentioned above contain different number of voxels with the same volume resolution.

Table 6.1 "Happy Buddha" model in four voxelized structure type with225×550×225 volume resolution.

	Single Shell	Multi- Level	Irregular Multi- Level	Full Volume
Voxel Number	2.5×10^6	2.8×10^7	3.2×10^6	2.8×10^7
Simulation Time	13ms	50ms	21ms	55ms

We demonstrate the "Happy Buddha" model in these methods with 225x550x225 volume resolution and the result shown in Table 6.2. All of these methods fully compute in parallel by GPU. We have only 10% voxel data comparing with fully volume resolution and 1.5 times faster than full volume structure. We record simulation time and compression rate with the voxel number of full volume structure in Figure 6.7 and 6.8.

We demonstrate "Max Planck" model for another example in Figure 6.9 and 6.10. The most different with "Happy Buddha" is the complexity of model shape. Our voxelized algorithm generates 8 layers with x axis, 14 layers with y axis and 8 layers with z axis in "Happy Buddha"; and generates 4 layers with x, 5 layers with y and 4 with z axis in "Max Planck". In the same volume resolution, the "Max Planck" model performs faster simulation time with less voxels.

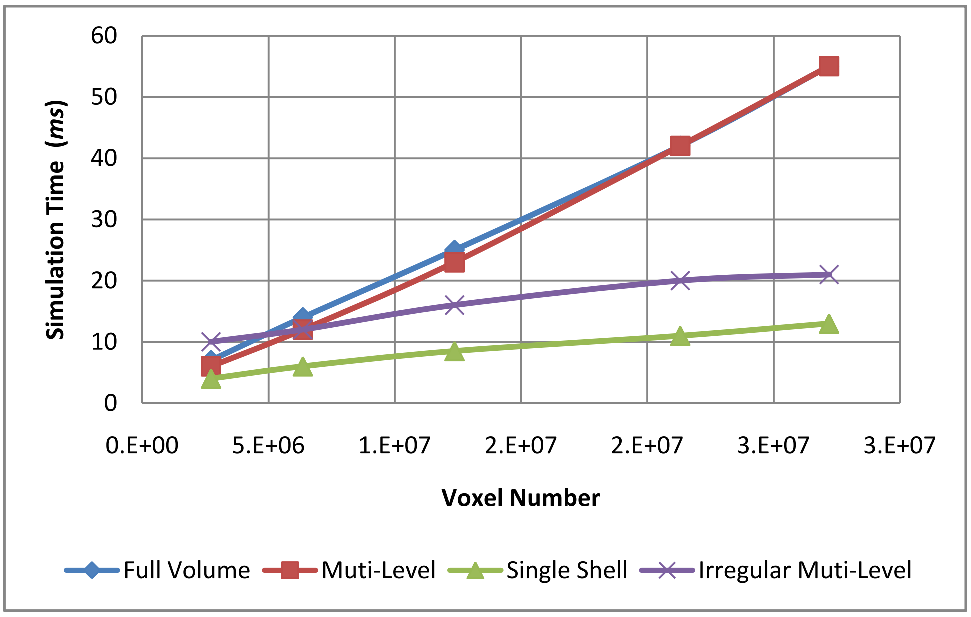

Figure 6.8 The simulation time of conduction in “Happy Buddha”.

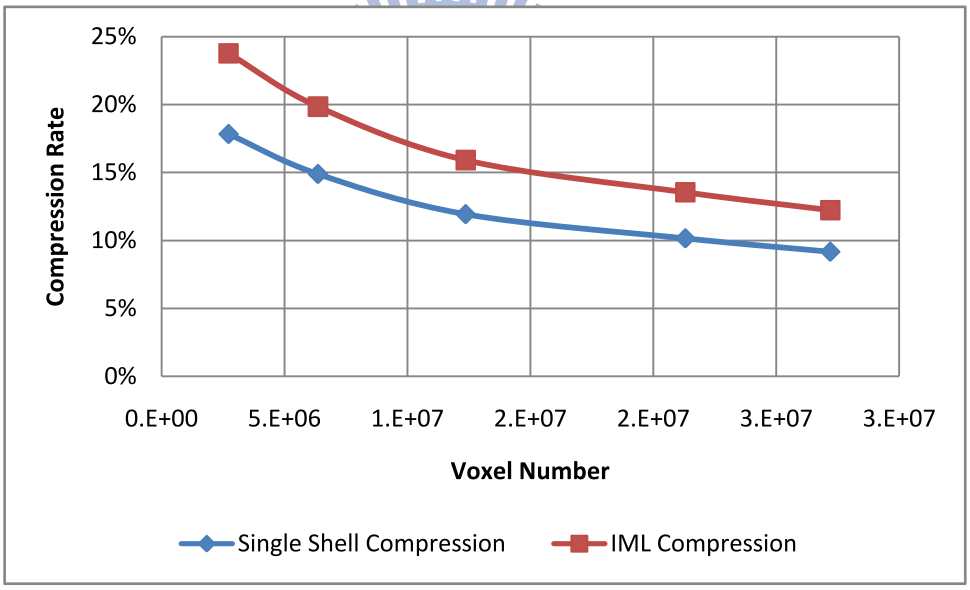

Figure 6.9 The voxel number compression rate of texture-based method, single shell and irregular multi-level, in “Happy Buddha” case.

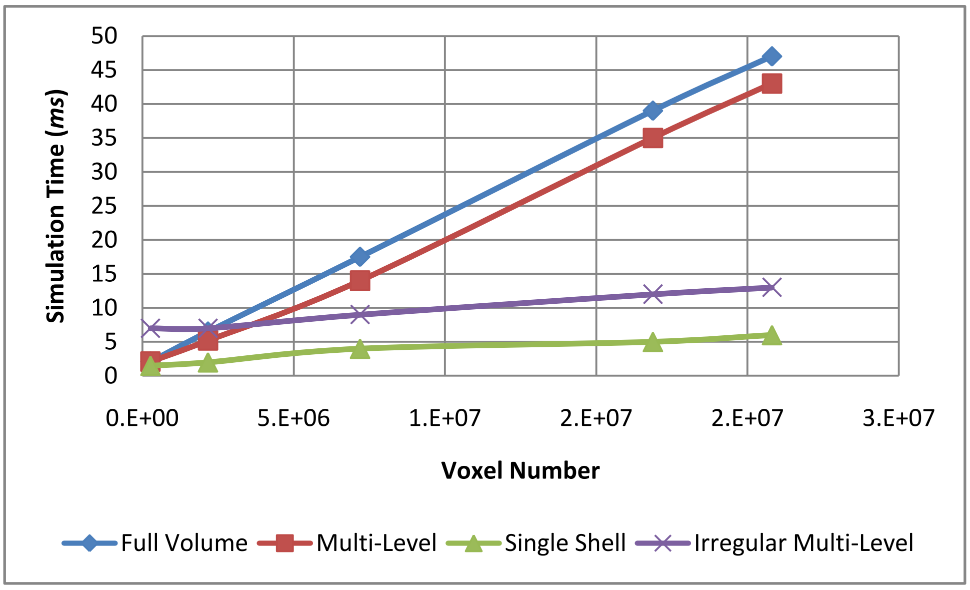

Figure 6. 10 The simulation time of conduction in “Max Planck”.

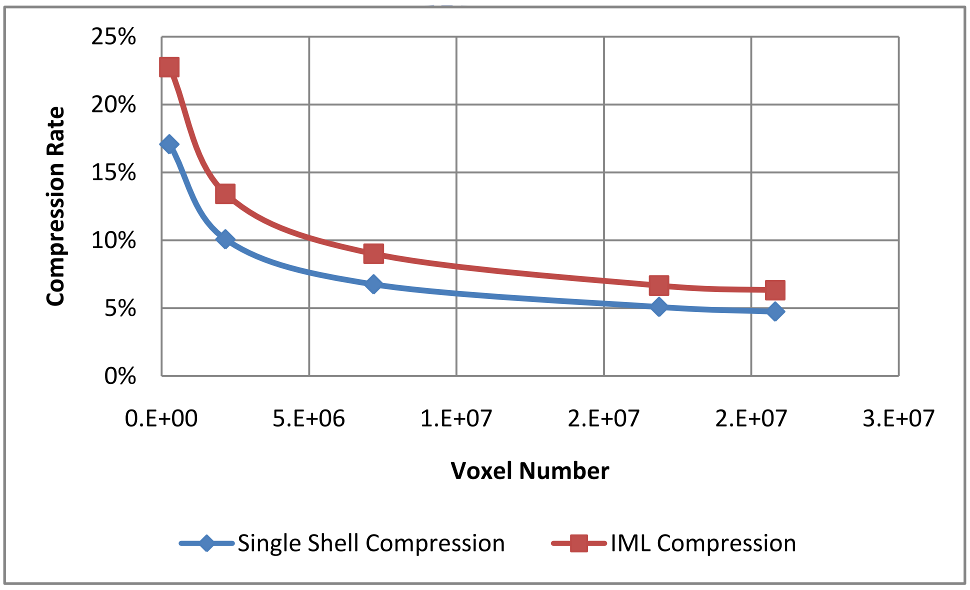

Figure 6.11 The voxel number compression rate of texture-based method in “Max Planck” case.

7. Conclusion

In this thesis, we present an approximation of heat transfer system consisting of radiation, conduction, convection and the producing visually similar thermal image. The process includes two main steps.

At first, we voxelize each object in the scene. Since the temperatures between various parts of object may not be the same, we apply finite element method to visualize temperature of object in detail. For this purpose, we separate surface of object model in orthogonal view and store geometric information to a series of textures.

Second, we approximate heat transfer. By this step, an object model can be represented as numerous voxels. Voxelized objects exchange heat with other voxels at contact under large temperature differences. We add wind blowing to make quickly temperature equilibrium of objects and environment. The voxelization textures store heat energy and update in parallel through GPU calculation. Finally, we render objects with stored heat in textures and reflected heat of radiation on surface in screen.

We provide an efficient framework implementation that fit into a general GPU-based visualization system. All of these methods are able to be accelerated by GPU-based rendering which synthesizes realistic thermal images of a virtual environment in real-time.

References

[BJO98] E. Buyruk, M. W. Johnson and I. Owen, “Numerical and experimental study of flow and heat transfer around a tube in cross-flow at low Reynolds number”, International Journal of Heat and Fluid Flow, Vol. 19(3), Pages 223-232, June 1998.

[Bunn05] M. Bunnell, “Dynamic Ambient Occlusion and Indirect Lighting”, *GPU Gems 2*, pages 223–233. Addison-Wesley, 2005.

[BWS99] G. Baciu, W. S. Wong and H. Sun, “RECODE: an Image-based Collision”, *Journal of Visualization and Computer Animation*, 10, 181–192, 1999.

[DS05] C. Dachsbacher and M. Stamminger, 2005, “Reflective shadow Maps”, Proceedings of the 2005 symposium on Interactive 3D graphics and games, ACM Press, New York, NY, USA, 203–231.

[Ever01] Everitt, C. “Interactive Order-Independent Transparency”, NVIDIA technical report, 2001.

[FBAF08] F. Faure, S. Barbier, J. Allard and F. Falipou, “Image-based Collision Detection and Response between Arbitrary Volume Objects”, *Eurographics/ ACM SIGGRAPH Symposium on Computer Animation*, 2008.

[FC00] S. Fang, H. Chen, “Hardware accelerated voxelization”, Computers and Graphics, Volume 24, Issue 3, Pages 433-442, June 2000.

[FKZQ*09] Z. Fan, Y. Kuo, Y. Zhao, F. Qiu and A. Kaufman, and W. Arcieri, “Visual simulation of thermal fluid dynamics in a pressurized water reactor”, Vis. Comput. 25, 11, Oct. 2009.

[GCFM*99]C. Garnier, R. Collorec, J. Flifla, C. Mouclier, F. Rousee, “Infrared sensor modeling for realistic thermal image synthesis”, Proceeding of Acoustics, Speech, and Signal Processing, IEEE International Conference, vol6, pp. 3513-3516, 1999.

[GTGB84] Goral, C. M., Torrance, K. E., Greenberg, D. P. and Battaile, B., “Modeling the Interaction of Light between Diffuse Surfaces”, *Computer Graphics, vol. 18, no. 3,* pp 213-222, 1984.

[GRLM03] N. K. Govindaraju, S. Redon, M. C. Lin and D. Manocha , “CULLIDE: Interactive Collision Detection Between Complex Models in Large Environments using Graphics Hardware”, *ACM SIGGRAPH/Eurographics Graphics Hardware,* 2003.

[HPH00] D. M. Harrild, R.C. Penland and C. S. Henriquez, “A flexible method for simulating cardiac conduction in three-dimensional complex geometries”, Journal of Electrocardiology , Vol. 33, Issue 3, Pages 241-251, July 2000.

[IDBL*06] Frank P. Incropera, David P. DeWitt, Theodore L. Bergman and Adrienne S. Lavine, “Fundamentals of Heat and Mass Transfer, 6th Edition”, Wiley, 6 edition, 2006.

[JWP03] Z. Jiang, Z. Wang and Q. Peng, “Real-Time Generation of Dynamic Infrared Scene”, in International Journal of Infrared and Millimeter Waves, 24(10): pp.1734-1748, Oct. 2003.

[JWJP04] Z. Jiang, Z. Wang, T. Zhou, J. Jin and Q. Peng, “Infrared image synthesis for bridges”, Proc. SPIE, Vol. 5405, 167, 2004.

[KCY06] W.A. Khan, J.R. Culham and M.M. Yovanovich, “Convection heat transfer from tube banks in crossflow: Analytical approach”, International Journal of Heat and Mass Transfer, Volume 49, Issues 25-26, December 2006, Pages 4831-4838.

[KHMS*98] J. T. Klosowski, M. Held, J. S. B. Mitchell, H. Sowizral and K. Zikan, “Efficient Collision Detection Using Bounding Volume Hierarchies of k-DOPs”, *appear in the March issue (Vol. 4, No. 1) of IEEE Transactions on Visualization and Computer Graphics*, 1998.

[Land02] H. Landis, “Production-ready global illumination”, *ACM SIGGRAPH*, Course: Notes 16, 2002.

[LFWK03] W. Li, Z. Fan, X. Wei and A. Kaufman, “Simulation with Complex Boundaries”, GPU Gems II, edited by Matt Pharr(Nvidia) and published by Addison Wesley, Chapter 47, Nov 2003.

[LWK03] W. Li, X. Wei and A. Kaufman, “Implementing lattice Boltzmann computation on graphics hardware”, The Visual Computer, Vol. 19, 7, pp. 444-456, Dec. 2003.

[Mitt07] MITTRING, M., “Finding next gen: Cryengine 2”, *ACMSIGGRAPH*, courses, 2007.

[MXJ08] J. Ma, Z. Xie and G. Jia, “Applying of Real-time Heat Transfer and Solidification Model on the Dynamic Control System of Billet Continuous Casting”, ISIJ International, Vol. 48, No. 12, pp. 1722–1727, 2008.

[Paly08] J.A. Palyvos, “A survey of wind convection coefficient correlations for building envelope energy systems' modeling”, Applied Thermal Engineering, Volume 28, Issues 8-9, June 2008, Pages 801-808.

[PCG] Research Images of Cornell University Program of Computer Graphics

http://www.graphics.cornell.edu/online/research/

[PR] P&R infrared

http://www.pr-infrared.com/videos/index.php

[RGS09] T. Ritschel, T. Grosch and H.P. Seidel, “Approximating Dynamic Global Illumination in Image Space”, *Proceedings of ACM SIGGRAPH Symposium on Interactive 3D Graphics and Games (I3D)*, 2009.

[Thermal Image] Thermography: thermal images of houses

http://www.salsatecas.de/x/thermography/house-thermal-imaging.htm

[WPLJ01] Z. Wang, Q. Peng, Y. Lu, and Z. Jiang, “A Global Infrared Image Synthesis Model for Large-Scale Complex Urban Scene”, in International Journal of Infrared and Millimeter Waves, Volume 22, Number 8, pp. 1193-1208, August 2001.

[WWBP01] Z. Wang, Z. Wu, H. Bao and Q. Peng, “Synthesis of infrared ground target and its background”, Proc. SPIE, Visualization and Optimization Techniques, volume 4553, 1, pages 173-178, 2001.

[XS99] H. Xue and C. Shu, "Equilibration of heat conduction simulation in a very thin film using molecular dynamics", International Journal of Numerical Methods for Heat & Fluid Flow, Volume 9, Issue 1, Page 60-71, 1999

[YWC07] J. Yang, Y. Wang and Y. Chen, “GPU accelerated molecular dynamics simulation of thermal conductivities”, Journal of Computational Physics, Volume 221, Issue 2, Pages 799-804, February 2007.

[ZIK98] S. Zhukov, A. Iones and G. Kronin, “An ambient light illumination model, *Proc. Eurographics Rendering Workshop*, 1998.